MEASUREMENT OF TRANSVERSE RELAXATION TIMES OF CEREBRAL METABOLITES IN BRAIN TUMORS

by

AKSHAY MADAN

Presented to the Faculty of the Graduate School of

The University of Texas at Arlington in Partial Fulfillment

of the Requirements

for the Degree of

MASTER OF SCIENCE IN BIOMEDICAL ENGINEERING

THE UNIVERSITY OF TEXAS AT ARLINGTON

August 2013

Acknowledgements

I would like to thank first Dr. Changho Choi for giving me a fantastic opportunity, for instigating, stimulating and motivating my research, for sharing his knowledge and experience and mentoring me to become an inquisitive researcher.

I would also like to thank Dr. Elizabeth Maher and Sarah McNeil for providing the patients without whom this thesis would not have been possible. I am grateful to Dr. Georgios Alexandrakis and Dr. Jimin Ren for accepting to be my thesis committee members. I have been very lucky to have lab members like Sandeep Kumar Ganji and Keith Hulsey. They provided me with an environment rich with questions and answers.

I would also like to thank my roommates and friends Vishal Subramani and Irfan Kerawalla for making my transition to USA and graduate school an easy one.

And finally, but hardy finally, I thank my parents Anil and Sangeeta Madan and my sister Aarushi Madan. It is because of their love, support and encouragement I am the person I am today.

July 22, 2013

Abstract

MEASUREMENT OF TRANSVERSE RELAXATION TIMES OF CEREBRAL METABOLITES IN BRAIN TUMORS

Akshay Madan, M.S.

The University of Texas at Arlington, 2013

Supervising Professor: Changho Choi

Proton (^{1}H) magnetic resonance spectroscopy (MRS) provides a non-invasive means of assessing metabolite concentration for a range of biologically important cerebral compounds *in vivo.* To extract quantitative information, additional data regarding proton spin relaxation phenomena is critical. Transverse relaxation times (T_2) of cellular metabolites depend on the local molecular environment in which they reside. Several neurological diseases alter the molecular environment, which may be reflected in the changes of the T_2 relaxation times. Therefore alterations in T_2 in tumors may provide important information about the local environment and a potential non-invasive diagnostic tool.

Thirty-seven adult patients with gliomas and 11 healthy volunteers were enrolled in the study. The tumors comprised 22 low grade (grade II) and 15 high grade (grade III and grade IV) gliomas. Proton T_2 relaxation times of the MRS signals of total NAA (tNAA) (2.01 ppm), total creatine (tCr) (3.03 ppm), and total choline (tCho) (3.2 ppm), were measured *in vivo* at 3T. The T_2 relaxation time of lactate (at 1.3 ppm) was measured in the 7 glioma patients in which the signal was well detectable. Single voxel localized point resolved spectroscopy data were acquired at 8 echo times (TE's = 58, 88, 118, 148, 178,

208, 238, and 268 ms). T_2 was obtained with monoexponential fitting of metabolite signal estimates vs. TE's.

The measured T_2 relaxation times of tCr and tCho were significantly different between tumor (171 ms and 297 ms respectively) and contra-lateral normal brain regions (152 ms and 244 ms respectively) but for tNAA (295 ms in tumors and 294 ms in contra-lateral normal brain) no significant difference was observed. For normal brain, low grade and high grade tumors, the mean tCr T_2 values were estimated to be 149 ± 8 ms, 165 ± 22 ms and 180 ± 32 ms, and the mean tCho T_2 values were measured as 255 ± 29 ms, 291 ± 32 ms and 305 ± 58 ms respectively. The tCr and tCho T_2 values in low grade ($p < 0.002$ and $p < 0.001$ respectively) and high grade tumors ($p < 0.0001$ and $p < 0.001$ respectively) were significantly different than in normal brain, but the difference between low and high grades was not significant ($p > 0.05$). For tNAA the mean T_2 was estimated to be 286 ± 41 ms, 276 ± 33 ms and 247 ± 28 ms in normal brain, low grade and high grade tumors respectively. The tNAA T_2 was significantly different between high grade tumors and normal brain ($p < 0.04$) as well as between low grade and high grade tumors ($p < 0.02$). This study reports the T_2 of lactate in tumors for the first time, which was measured to be 256 ± 22 ms. Absolute quantification of lactate as well as tCr, tCho and tNAA was performed using the measured T_2 relaxation times.

Table of Contents

List of Illustrations

Figure Page

Chapter 1

Background and Introduction

The phenomenon nuclear magnetic resonance (NMR) was first observed in the early 1930's [1] and has since found many applications in the fields of chemistry, physics, biology and medicine. Proton (^{1}H) magnetic resonance spectroscopy (MRS) provides a non invasive tool for measuring metabolites in the human brain and has been extensively used to study brain tumors [2-6].

1.1 Spin

NMR exploits the spin property of atomic nuclei. Nuclei with spin (I) = ½ can easily be examined by NMR experiments [7]. Along with ^{1}H, other nuclei with spin (I) = ½ are ^{13}C, ^{15}N, ^{19}F, ^{29}Si, ^{31}P. A spin (I) = ½ can exist in one of two energy states, i.e. |+½> or |-½>. The + ½ energy state is a lower energy state and vice versa. The splitting into two energy levels in the presence of a magnetic field is called the Zeeman Effect. This energy difference ΔE is given by the equation

$$\Delta \boldsymbol{E} = \hbar\, \boldsymbol{\omega_0} = \boldsymbol{h}\, \boldsymbol{v_0} = \hbar\, \boldsymbol{\gamma}\, \boldsymbol{B_0} \qquad [1\text{-}1]$$

where $\hbar$ is the Planck's constant divided by 2π, ω_0 (= $2\pi \boldsymbol{v_0}$) is the Larmor frequency, γ is the gyromagnetic ratio and B_o is the external magnetic field.

The population difference between the two energy states at thermal equilibrium is given by

$$\frac{\boldsymbol{n}\left(\pm\frac{\boldsymbol{1}}{\boldsymbol{2}}\right)}{\boldsymbol{n}\left(\mp\frac{\boldsymbol{1}}{\boldsymbol{2}}\right)} = \boldsymbol{exp}\left(\frac{-\Delta \boldsymbol{E}}{\boldsymbol{kT}}\right), \qquad [1\text{-}2]$$

where n is the number of spins in the particular energy state, ΔE is the energy difference between the spin states, k is the Boltzmann's constant and T is the absolute temperature in Kelvin.

In a sample at room temperature, due to the effect of thermal energy, the number of spins in the lower energy state is slightly larger than the higher energy state. The bulk magnetization resulting from the population difference, i.e. the sum of the magnetic moments of spins in the sample, is aligned along the external magnetic field. The equation for the bulk magnetization M_0 at thermal equilibrium is given by

$$M_0 = \left(\frac{\gamma h}{2\pi}^2\right) \frac{NB_0}{4kT} \qquad [1\text{-}3]$$

where N is the total number of spins in the sample.

1.2 Excitation and Detection

The direction of the applied static magnetic field B_0, is defined as the Z direction. The magnetization along this direction is called the longitudinal magnetization (i.e. $M_0 = M_z$). In order to observe the NMR signal the magnetization M_0 has to be tipped to the transverse plane, perpendicular to B_0. To achieve this, a radio frequency (RF) field (B_1) is applied at the Larmor frequency. The spins then absorb energy from the applied RF field and as a result the equilibrium populations of the two energy states are perturbed [8]. The external RF gives rise to the formation of a transverse magnetization, which rotates about B_0 at the Larmor frequency. This rotating magnetization is recorded in the time domain using an RF coil.

1.3 Chemical Shift

In NMR the resonance frequency of a nucleus depends on the gyromagnetic ratio γ, the external magnetic field B_o, and the chemical environment within the molecule (chemical shift). The magnetic field B experienced by the nucleus is influenced by the interaction between the surrounding electron cloud and the external field B_o. This effect is termed as shielding, σ. The effective external field experienced by the nucleus is given by

$$B = B_0(1 - \sigma) \quad [1\text{-}4]$$

The equation for resonance frequency can now be written as

$$\vartheta = \frac{\gamma}{2\pi} B_0(1 - \sigma) \quad [1\text{-}5]$$

Chemical shift is defined as

$$\delta = \frac{\vartheta - \vartheta_{ref}}{\vartheta_{ref}} \times 10^6 \quad [1\text{-}6]$$

where ϑ is the resonant frequency of the nucleus under investigation and $\vartheta_{ref}$is the resonant frequency of the reference compound. Chemical shifts are usually expressed in parts per million (ppm). For ^{1}H NMR studies the compound tetramethylsilane (TMS) is commonly used as reference and is assigned a chemical shift value of 0 ppm.

1.4 Slice selection

An *in vivo* MRS experiment is commonly undertaken with spatial localization. Single-voxel localization can be obtained with three orthogonal slice selections. Slice selection is achieved by the combination of an RF pulse and a magnetic field gradient, as shown in Figure 1-1. When a magnetic field gradient pulse is applied in a particular direction (e.g., z direction), a linear distribution of rotational frequency is created along that direction. A frequency selective RF pulse applied during the magnetic field gradient pulse excites only those nuclei within the selected volume (shaded volume in the figure). The position of the slice is determined by the magnetic field gradient strength and the carrier frequency of the RF pulse. The thickness of the slice selected is determined by the magnetic field gradient strength and the excitation bandwidth of the RF pulse.

The equation for slice thickness can be written as

$$\Delta \boldsymbol{Z} = \frac{\Delta \boldsymbol{\omega}}{\boldsymbol{\gamma G_z}} \quad [1\text{-}7]$$

where ΔZ is the thickness of the slice, $\Delta\omega$ is the bandwidth of the RF pulse, and G_z is the magnetic field gradient strength.

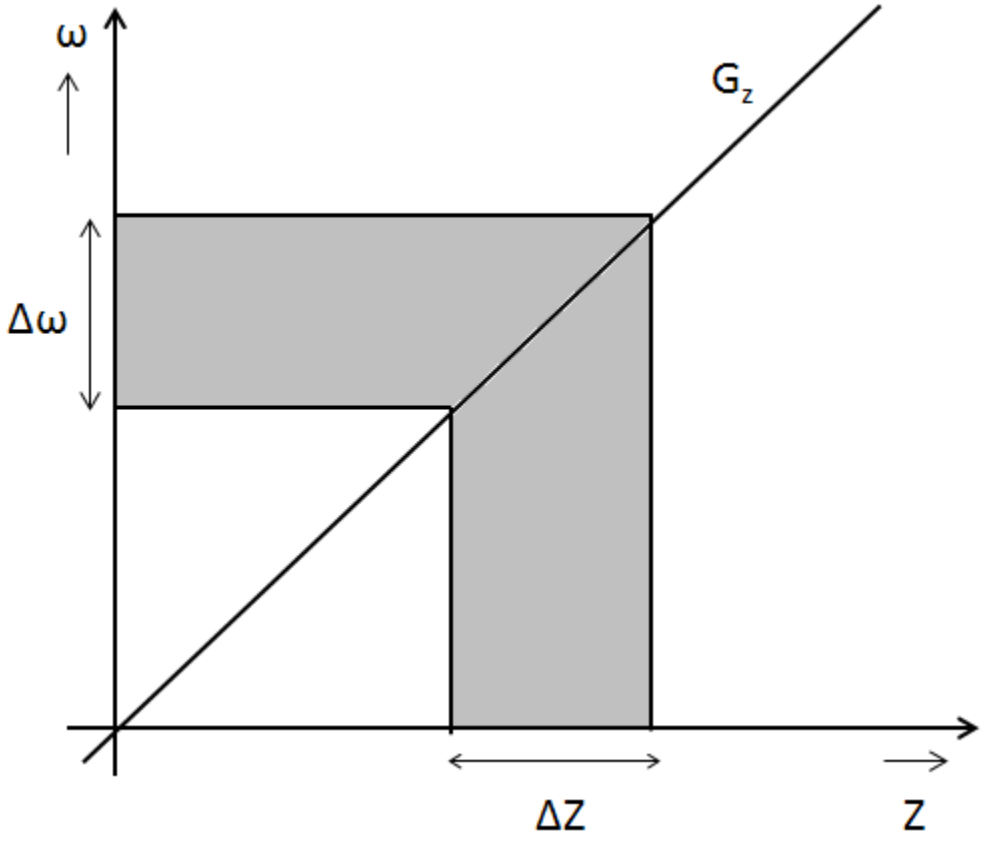

Figure 1-1 A schematic diagram for slice selection. When a magnetic field gradient pulse G_z is applied in the Z direction during an RF pulse with bandwidth $\Delta\omega$ the spins within the slice of thickness ΔZ are excited. The slice thickness is determined by the bandwidth $\Delta\omega$ and magnetic field gradient strength G.

1.5 Single-voxel localized MRS

The most commonly used single-voxel localized MRS sequences are point resolved spectroscopy (PRESS) and stimulated echo acquisition mode (STEAM).

1.5.1 Point resolved spectroscopy (PRESS)

Figure 1-2 shows the PRESS sequence which consists of a slice selective 90° RF pulse and two slice selective 180° RF pulses. Each of these pulses is applied simultaneously with a field gradient pulse. The 90° pulse tips the magnetization to the transverse plane and the 180° pulse refocuses the transverse magnetization. Spoiler gradients are applied symmetrically with respect to 180° pulses to dephase the signals from outside the volume of interest. An echo at time $TE_1 + TE_2$, which is generated from an overlapped volume of the three slices defined by the 90° and 180° RF pulses, is recorded.

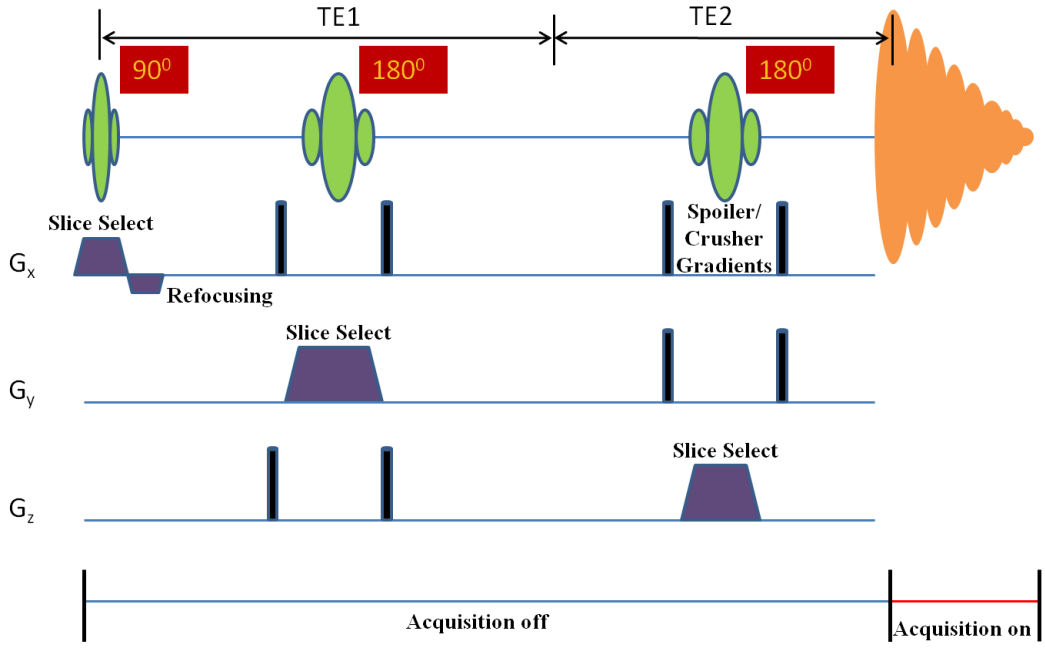

Figure 1-2 Schematic diagram of a point resolved spectroscopy (PRESS) sequence.

1.5.2 1.5.2 Stimulated echo acquisition mode (STEAM)

A STEAM sequence consists of three slice selective 90° RF pulses, as shown in Figure 1-3. A stimulated echo is formed at time TE+TM (mixing time), which is at a time

TE/2 after the third 90° pulse. The signal intensity in STEAM is half as compared to PRESS.

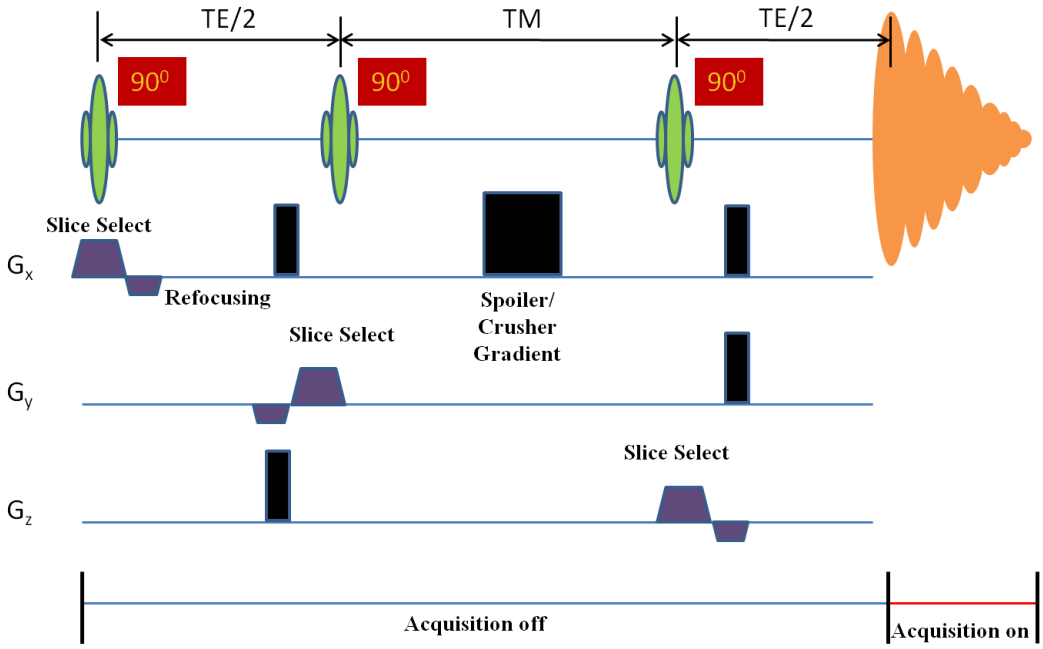

Figure 1-3 Schematic diagram of a stimulated echo acquisition mode (STEAM) sequence.

1.6 Water suppression

Suppression of water signal is required for obtaining the brain metabolite signals (the brain water concentration is greater than 40 molar whereas the metabolite concentrations are on the order of millimolar). In the majority of spectroscopy data acquisitions water suppression is done in the preparation phase before localization is performed. Water suppression is achieved by applying spectrally selective RF pulses and dephasing gradient pluses.

1.7 Relaxation

As explained in section 1.1, at the thermal equilibrium the population of the spins in the two energy states is distributed in accordance with the Boltzmann's distribution and

there is no transverse magnetization. The application of an RF pulse perturbs the spins into a non-equilibrium state. The process by which the spins return to equilibrium is called relaxation.

1.7.1 Longitudinal Relaxation

Longitudinal relaxation (T_1), often referred to as spin-lattice relaxation, is the mechanism by which the longitudinal magnetization returns to its state of thermal equilibrium by releasing the absorbed RF energy to the lattice. Following the excitation of the spins by a 90° pulse the longitudinal magnetization recovers exponentially as described in equation 1-8.

$$M_Z = M_0 \left(1 - e^{\frac{-t}{T_1}}\right) \quad [1\text{-}8]$$

where M_z is the longitudinal magnetization at time t, M_0 is the magnetization at thermal equilibrium and T_1 is the time during which the z component of the magnetization is recovered to 0.63 times (or 1 - e^{-1}) the thermal equilibrium magnetization.

1.7.2 Transverse Relaxation

Transverse relaxation (T_2), often referred to as spin-spin relaxation, is the loss of coherence of spins in the transverse plane following an excitation. The transverse magnetization M_{xy} decreases with time. T_2 is defined as the time during which the transverse magnetization reduces to 1/e of the M_{xy} at zero TE, as shown in Figure 1-4.

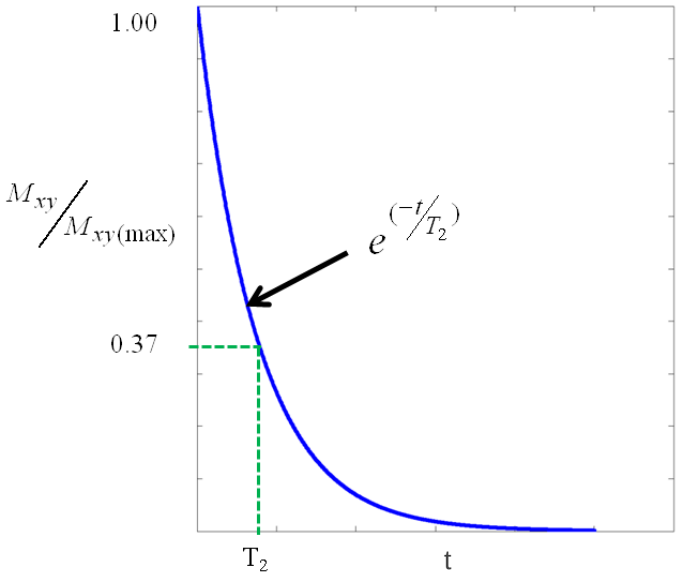

Figure 1-4 T_2 relaxation curve. The transverse magnetization decays exponentially towards its equilibrium value of zero. At time T_2 the magnetization has decayed to 37% (=1/e) of its initial value.

.

Immediately after a 90° pulse is applied, spins begin to dephase with time due to the interaction with each other and thus the observed signal decays exponentially according to the equation

$$M_{xy} = M_0 \left(e^{\frac{-t}{T_2}} \right) \qquad [1\text{-}9]$$

Fluctuations in the magnetic field at the nucleus can cause T_2 relaxation. The primary source of fluctuating magnetic fields is molecular motions. There are several mechanisms for relaxation: dipole-dipole interactions, quadrupole interactions, chemical shift anisotropy effects, scalar (spin-spin coupling) and spin-rotation effects [9].

The dipole-dipole interaction is the most dominant relaxation mechanism in ^{1}H MRS. Dipole-dipole interactions occur when two spins that are close to each other in space experience each other's magnetic field, which leads to a slightly different effective magnetic field B_{eff} at one spin that depends on the orientation of both magnetic dipoles.

The strength of the dipole-dipole coupling depends on the spin-spin distance r and the angle φ formed by the vector between the two nuclei. The equation for the effective magnetic field experienced by the spin is given by [9]

$$B_{eff} = \frac{\mu\,(3cos^2\,\varphi - 1)}{r^3} \qquad [1\text{-}10]$$

Through molecular tumbling the angle φ changes, thus changing the magnitude of the magnetic field B_{eff} causing a fluctuating magnetic field.

The Bloembergen, Purcell, Pound (BPP) theory describes the relaxation times in terms of correlation times ($\boldsymbol{\tau}_c$) and spin-spin distance r [10]. The correlation time is defined as the average time it takes a molecule to rotate over one radian.

According to the BPP theory the T_2 relaxation is given by [10]

$$\frac{1}{T_2} = \frac{K}{2}\left[3\tau_c + \frac{5\tau_c}{\left(1+\omega_0{}^2{}_0\tau_c{}^2\right)} + \frac{2\tau_c}{(1+4\omega_0{}^4{}_0\tau_c{}^4)}\right] \qquad [1\text{-}11]$$

where

$$\tau_c = \frac{4\pi\eta a^3}{3kT} \qquad [1\text{-}12]$$

and

$$K = \frac{3\mu^2\hbar^2\gamma^4}{160\pi^2 r^6} \qquad [1\text{-}13]$$

where η is the viscosity and a is the molecular radius.

Correlation time is a quantitative measure of the rate of a molecular motion. The correlation time is long in molecules moving slowly and short when molecules move rapidly. The correlation time increases with increasing size of the molecules. Liquids have a very short τ_c ≈ 10^{-12} seconds. The Figure 1-5 shows the relationship of transverse relaxation with correlation time.

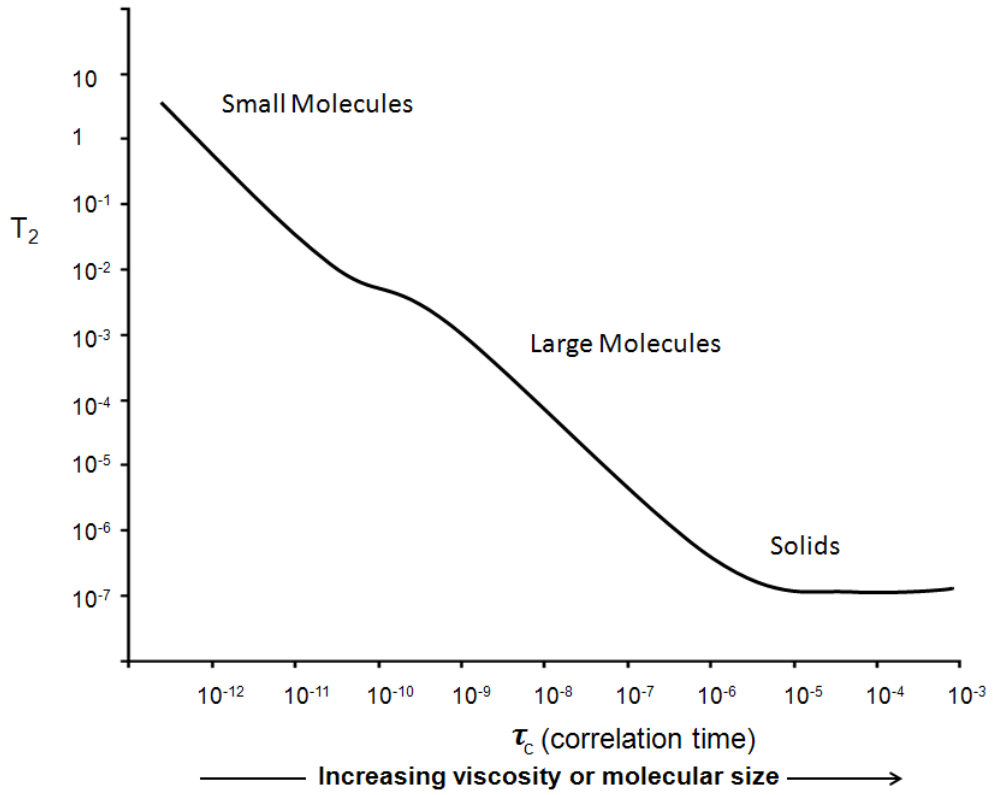

Figure 1-5 The dependence of transverse relaxation time T_2 on the correlation time (τ_c).

With increase in the correlation time the spins experience fields from the surrounding spins longer, which leads to faster relaxation of the transverse magnetization thus reducing the T_2. The transverse relaxation time also decreases with increasing viscosity or molecular size.

The transverse relaxation time of metabolites depends on the molecular mobility, which may be altered in neurological diseases. The resulting changes in the transverse relaxation time of metabolites may provide insight into molecular mechanisms of disease progression. For example, short T_2 may indicate increased restriction of molecular movement whereas long T_2 may indicate that the molecules can move freely [11].

Previous studies have reported changes in T_2 in diseases such as Parkinson's [12], Huntington's [13], schizophrenia [14, 15] and bipolar disorder [15], lending support to investigating T_2 changes in other diseases such as brain tumors.

Chapter 2

Brain Tumors

A brain tumor is an abnormal growth of tissue in the brain or the central spinal canal. There are two types of tumors: benign and malignant. Benign tumors are non-cancerous; they do not recur and do not spread to other parts of the body. Even though benign tumors may not be life threatening they can potentially progress to become malignant. Malignant tumors grow rapidly and can recur even after resection unless treated adequately.

Brain tumors can be primary or secondary. Primary brain tumors can be benign or malignant but secondary brain tumors are malignant in most cases. The World Health Organization (WHO) classification system is most commonly used to classify tumor type and grade [16]. This system classifies tumors according to the origin and behavior of the cells. Several tumor types are assigned a grade from I to IV to signify the rate of growth, with I being the least malignant and IV being most malignant.

2.1 Types of brain tumors

Brain tumors are divided into two types: gliomas and non glial brain tumors. Gliomas as the name suggests arise from the glial cells. The most common type of gliomas are

i. Astrocytomas
ii. Oligodendrogliomas
iii. Ependymomas
iv. Oligoastrocytomas

2.1.1 Astrocytomas

Astrocytomas originate from the star shaped glial cells called astrocytes. Astrocytomas can occur in many parts of the brain especially in the cerebrum and usually

do not spread outside the brain and spinal cord. Astrocytomas can develop in children as well as in adults.

Astrocytomas are classified into one of three types according to their grades (i) low grade astrocytomas (Grade II), (ii) anaplastic astrocytomas (Grade III) and (iii) glioblastoma multiforme (GBM) (Grade IV)

2.1.1.1 Low grade astrocytomas (Grade II)

Low grade astrocytomas are slow growing gliomas. They account for 10 percent of adult astrocytomas and the majority of pediatric brain tumors. They are usually benign but can progress to a malignant glioma. Low grade astrocytomas are invasive i.e. they penetrate into the surrounding normal tissue. Due to this nature they can easily recur. Treatment depends on the tumor location and size. If the tumor is in an accessible location it is resected. Follow-up imaging scans are undertaken every few months to monitor for recurrence. Radiation may be suggested post surgery. Radiation may also be suggested for tumors which cannot be safely resected (e.g., brainstem).

2.1.1.2 Anaplastic astrocytoma (Grade III)

Many low grade astrocytomas progress to anaplastic astrocytomas. The most common symptoms are headache, depressed mental status, focal neurological defects and seizures. The typical course of treatment for anaplastic astrocytomas is resection of the tumor as much as possible followed by radiation therapy. Chemotherapy with temozolomide as an adjuvant to radiation is also used, especially in cases of recurrence.

2.1.1.3 Glioblastoma multiforme (GBM) (Grade IV)

Glioblastoma multiforme is the most common and most malignant primary brain tumor. GBM develops primarily in the cerebral hemispheres but it can also develop in other parts of the brain, brainstem or spinal cord. GBM can develop from progression of lower grade astrocytomas or directly from glial cells. The median survival rate is 15

months. Complete resection is impossible in most cases as GBM tumors infiltrate the normal surrounding brain tissue. Standard treatment is resection (of the tumor as much as possible) followed by radiation or combined radiation therapy and chemotherapy.

2.1.2 Oligodendrogliomas

Oligodendrogliomas originate from the oligodendrocytes of the brain. They can be low grade (grade II) or high grade (grade III or anaplastic). They can occur anywhere within the cerebral hemisphere but most commonly occur in the frontal and temporal lobes. The treatment for low grade is resection followed by radiation if there is residual tumor post resection. High grade tumors are treated with a combination of radiation and chemotherapy post resection. Their cause has been linked to chromosomal abnormalities which may play a role in their development.

2.1.3 Oligoastrocytomas

Oligoastrocytomas are often called mixed gliomas. They originate from both oligodendrocytes and astrocytes and have characteristics of both type of tumors (oligodendrogliomas and astrocytomas). They can be low grade or anaplastic. Treatment is determined based on the most anaplastic type of cells found in the tumor. For example, if the tumor is composed of an anaplastic astrocytoma and low grade oligodendroglioma then the treatment would be based on anaplastic astrocytoma which is the more aggressive of the two.

2.2 Brain metabolites

Brain metabolites that are most commonly measured using MRS are N-acetylaspartate (NAA), creatine (Cr), choline containing compounds (Cho), myo-inositol (mIns), glutamate (Glu), glutamine (Gln), lactate (Lac), and γ-aminobutyric acid (GABA). These metabolites are altered in tumors.

2.2.1 N-acetylaspartate (NAA)

NAA is considered to be a neuronal marker and is reduced in many diseases like multiple sclerosis, brain tumors, infarcts, etc, which are accompanied by neuronal loss. Measurement of NAA may be useful for assessment of neuronal ‘’health’’ or integrity in the central nervous system [17]. NAA is localized in the central and peripheral nervous system. The concentration varies in different parts of the brain [18] and also changes with developmental changes, increasing from birth to adulthood [19]. The NAA concentration is markedly reduced in tumors due to displacement and destruction of normal tissue. The NAA CH_3 protons resonating at 2.01 ppm, give rise to the largest signal in ^1H MRS in healthy brain. This NAA signal is overlapped by the N-acetylaspartylglutamate (NAAG) singlet resonating at 2.04 ppm. The NAA and NAAG signals are difficult to separate *in vivo*. The composite signal is often estimated and termed total NAA (tNAA). The tNAA concentration in healthy brain is in the range of 10 – 15 mM.

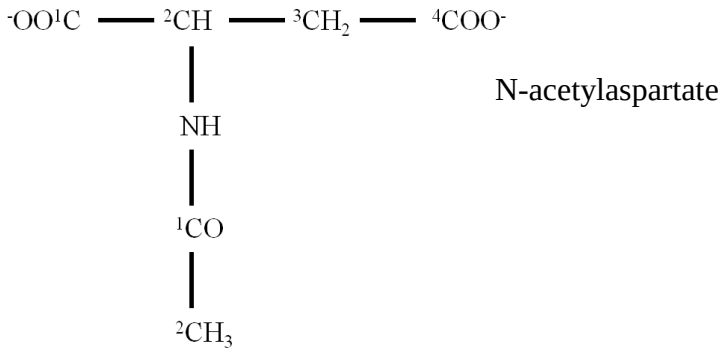

Figure 2-1 Chemical structure of NAA.

2.2.2 Creatine

Creatine (Cr) plays a major role in energy metabolism via the creatine kinase reaction, which generates ATP (adenosine triphosphate). Creatine shows large regional variations, with lower levels in white matter than gray matter in normal brain, as well as very high levels of Cr in the cerebellum [20]. No changes in creatine concentrations have

been reported with age [21] and in a variety of diseases. Creatine is reduced in high grade gliomas, metastases and meningiomas [22, 23]. Previous studies have also reported that creatine is elevated in astrocytomas followed by progressive reduction with increase of anaplasia [24-26]. The methyl resonance of creatine at 3.02 ppm is overlapped with the signal from phosphocreatine, therefore the signal is reported as total creatine (tCr). The CH_2 proton resonance of creatine is observed at 3.92 ppm. The tCr concentration in healthy brain is about 7 - 9 mM in gray matter and about 5 - 6 mM in white matter.

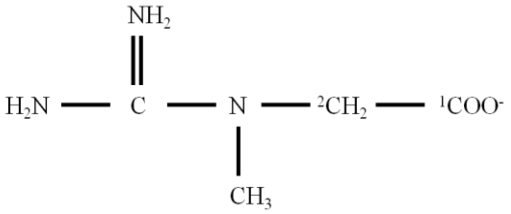

Creatine

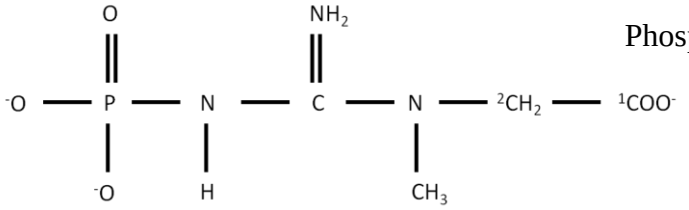

Phosphocreatine

Figure 2-2 Chemical structure of Cr and PCr.

2.2.3 Choline containing compounds

Total choline (tCho) detected at 3.2 ppm is a sum of the CH_3 proton signals of phosphocholine (PC), glycerophosphocholine (GPC) and free choline. Choline shows the largest regional variation in concentration of all the metabolites [18] and its concentration is larger in white matter than gray matter. The total choline concentration in healthy brain is about 1 – 2 mM. The primary contributions to the total choline signal are from PC and GPC. The contribution from free choline is very low because of its low concentration in

healthy brain but is significantly increased in tumors. Choline containing compounds are involved in membrane synthesis and degradation [17]. It is thought to be a marker of increased cell density and membrane turnover [27]. It is elevated in diseases like tumors, ischemia, head trauma, Alzheimer's disease, dementia and multiple sclerosis, and is reduced in stroke and liver disease. Elevated tCho has been recognized as an important surrogate marker of tumor progression [24].

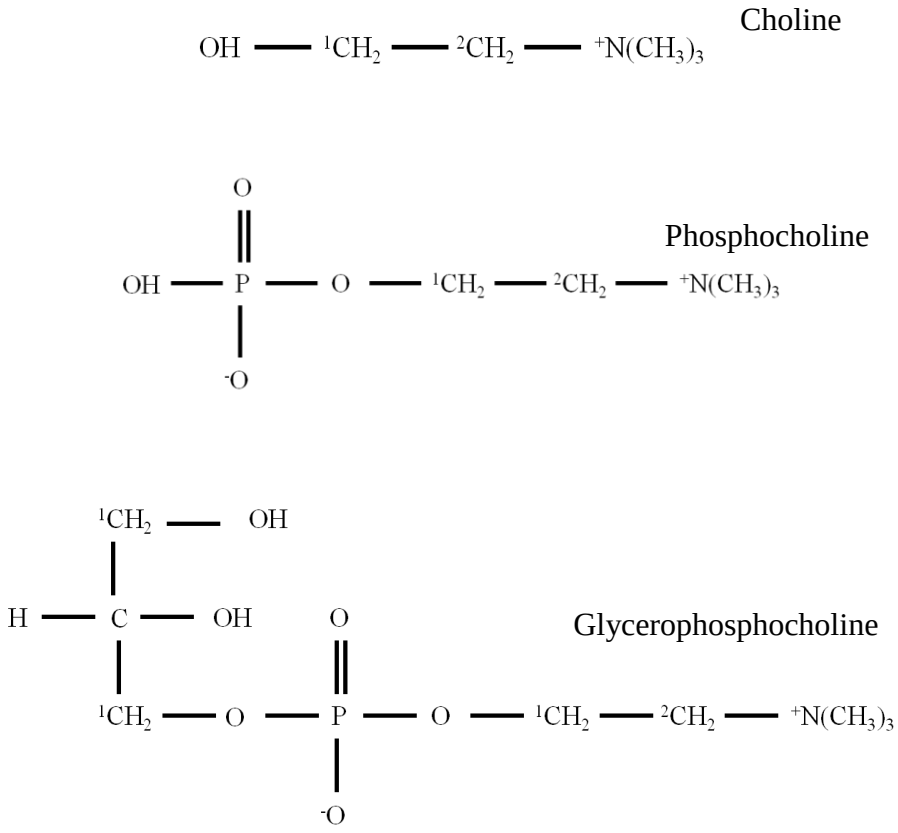

Figure 2-3 Chemical structure of free Cho, PC and GPC

2.2.4 Lactate

Lactate is present in normal brain at relatively low concentrations (< 1 mM). The concentration is elevated in several diseased conditions. Lactate has been extensively studied because of its potential use in clinical diagnosis. Anaerobic glycolysis occurring during diseased conditions leads to increased local concentration of lactate [28].

Reduced clearance rate of lactate in necrotic or cystic regions is another reason for increased lactate concentration [29]. The CH_3 and CH protons of lactate resonate at 1.3 and 4.1 ppm, with a J coupling strength of 7 Hz, as shown in Figure 2-4. Due to the effects of its coupling to the CH proton, the prominent resonance at 1.3 appears as a doublet at short echo times. Since this doublet is overlapped with the lipid signals, lactate is often measured using long echo times, e.g., TE = 140 ms (= 1/J), at which the lactate 1.3 ppm signal becomes an inverted doublet while lipid signal remains positive and is markedly attenuated due to the short T_2 of lipids [30]. In order to accurately estimate the lactate concentrations from long TE sequences, it is essential to correct for the T_2 relaxation effects. Therefore it is important to measure the T_2 of lactate to obtain zero-TE magnetization which is directly proportional to the concentration.

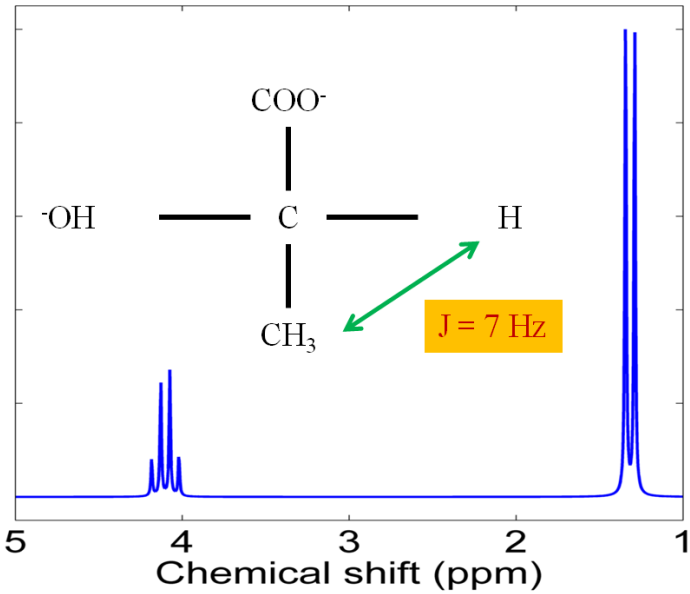

Figure 2-4 Chemical structure and the ^1H spectra of lactate. The CH_3 and CH resonances (at 1.31 and 4.09 ppm respectively) are J coupled with a strength of 7 Hz.

Chapter 3

Materials and Methods

3.1 Patient Information

Thirty seven patients with gliomas (age range 25 – 80, median 39; 22 males and 15 females) and 11 healthy volunteers (age range 21 – 50, median 27; 6 males and 5 females) were recruited to undergo brain MRS scans. Of the 37 glioma patients, 13 were diagnosed with oligodendroglioma, 9 with low grade gliomas, 6 with anaplastic oligodendroglioma, 4 with anaplastic astrocytoma, 2 with anaplastic oligoastrocytoma and 3 with glioblastoma. The tumor types were determined by the histopathological analysis on surgical biopsy according to the WHO criteria except for the 9 low grade gliomas which were diagnosed by clinicians based on clinical MRI data and increased 2-hydroxyglutarate [31] which occurs in isocitrate dehydrogenase (IDH) mutated gliomas [32].

The tumor data were divided into two groups according to their grade (a) low grade (b) high grade. Oligodendroglioma and low grade gliomas were classified as low grade (grade II) gliomas whereas anaplastic oligodendroglioma, anaplastic astrocytoma, anaplastic oligoastrocytoma and glioblastoma were classified as high grade.

3.2 Experimental Design

All MR experiments were carried out on a whole-body 3T scanner (Philips Medical Systems, Best, The Netherlands) using a body coil for RF transmission and an 8-channel phased-array head coil for signal reception. The data were acquired using a PRESS [33] sequence with the following RF pulse and delay order: 90 – $TE_1/2$ – 180 – $TE_1/2$ – $TE_2/2$ – 180 – $TE_2/2$ – acquisition, as shown in Figure 3-2.

3.2.1 Imaging

The location of tumor was indentified with T_2 – weighted fluid attenuated inversion recovery (T_2w FLAIR) imaging, which nulled the signal from cerebrospinal fluid (CSF) via an inversion recovery time (TI) and allowed non-CSF tissues adequate signal recovery before readout. With nulling of the CSF, long-TE readout was used to increase T_2 weighting hence improving the conspicuity of most tissue abnormalities without the deleterious effects of CSF signals [34]. The T_2w FLAIR imaging parameters included: repetition time (TR) = 11000 ms, echo time (TE) = 125 ms, TI = 2800 ms, acquisition matrix size of 352 x 212, imaging time of 3 min and 40 sec.

3.2.2 Spectroscopy

3.2.2.1 Phantom Experiments

Experiments were carried out on a GE “Braino” phantom (GE Medical Systems, Milwaukee, WI, USA) containing metabolites such as N-acetylaspartate (12.5 mM), creatine (10.0 mM), choline (3.0 mM), glutamate (12.5mM), myo-inositol (7.5 mM) and lactate (5.0 mM). Data were acquired using a PRESS sequence at TE’s = 58, 88, 118, 148, 178, 208, 238 and 268 ms. The voxel size was 25 x 25 x 25 mm^3 and TR was 6 sec. The number of sampling points (FID) was 2048 with a spectral width of 2500 Hz. The RF carrier pulse was set at 2.5 ppm. A four pulse variable flip angle scheme was used for water suppression. The data were acquired with 4 averages at each echo time and two averages for unsuppressed water data.

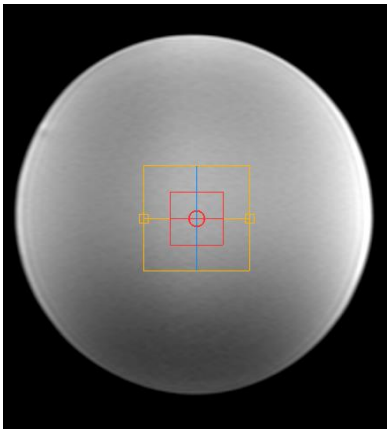

Figure 3-1 GE Braino phantom. Scout image in the axial orientation. The yellow box is the shim volume and the red box is the volume of interest (PRESS localized volume).

3.2.2.2 *In Vivo* Experiments

In vivo experiments were performed on 11 healthy volunteers and 37 tumor patients. Written informed consent was obtained prior to each of the *in vivo* scans. The protocol was approved by the Institutional Review Board of the University of Texas Southwestern Medical Center. For normal brains, data were obtained from the right parietal cortex and medial occipital regions which were predominantly white and gray matter regions, respectively whereas in tumor patients the data were obtained from the T_2w FLAIR hyperintensity region. A PRESS sequence was used for data acquisition at TE's = 58, 88, 118, 148, 178, 208, 238 and 268 ms. After data acquisition for metabolites, unsuppressed water data were acquired with the same pulse sequence and gradients as metabolite data. The voxel size was 20 x 20 x 20 mm^3 and TR = 2 sec. Volume localization was achieved using a 9.8 ms amplitude/frequency modulated 90° RF pulse (bandwidth = 4.25 kHz) and two 13.2 ms amplitude modulated 180° RF pulse (bandwidth = 1.27 kHz) with carrier frequencies at 2.5 ppm. An RF field intensity (B_1) of 13.5 μT was used for the RF pulses. A four pulse variable flip angle scheme was used for water suppression [35]. A 64 step phase cycling scheme was used. First and second order

shimming for the selected volume was carried out using the fast automatic shimming technique by mapping along projections (FASTMAP) [36]. The data were acquired, at each echo time, with 16 averages for water-suppressed metabolite data and with two averages for unsuppressed water data.

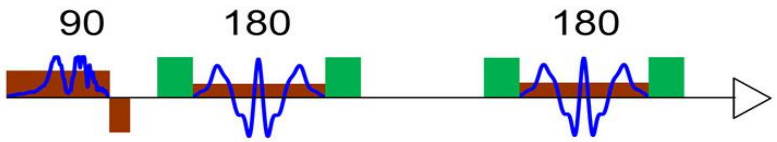

Figure 3-2 PRESS sequence with the 90° and two 180° RF pulses used in this study. The slice selective gradients are shown in brown and the spoiler gradients are shown in green.

3.2.2.3 Data Analysis

The data acquired at each echo time were post-processed for residual water suppression, eddy current correction, frequency drift correction and zero and first order phase correction. Residual water signal was suppressed using the HLSVD algorithm of the jMRUI® software package [37].The other post-processing steps were performed using in house written Matlab programs. Eddy current artifacts in the metabolite data were minimized by correcting the phase of the data points of the free-induction decay (FID) using the phase factor of the unsuppressed water FID signal. The data were zero filled to 4096 complex points. The frequency drifts were corrected using the NAA singlet as reference in normal brain data and the choline singlet as reference in tumor data. Data were apodized using a 2 Hz exponential function for enhancing SNR and removing potential artifacts in the later part of the FID. Spectral fitting was performed using the LCModel software [38]. The basis function for fitting included numerically calculated model spectra of 22 brain metabolites including N-acetylaspartate (NAA), creatine and phosphocreatine (tCr), glycerophosphocholine, phosphocholine and free choline (tCho),

lactate (Lac), 2-hydroxyglutarate (2HG), glutamate (Glu), glutamine (Gln), GABA, myo-inositol (mI), glycine (Gly), taurine (Tau), scyllo-inositol (sI), aspartate (Asp), phosphorylethanolamine (PE), serine (Ser), ethanolamine (Eth), alanine (Ala), acetate (Ace), glucose (Glc), N-acetylaspartylglutamate (NAAG), glutathione (GSH) and citrate (Cit). The basis spectra were calculated including the effects of the PRESS volume-localizing RF and gradient pulses similarly as described in the Supplementary Information of a previous paper [31]. The spectral fitting was conducted between 0.5 and 4.1 ppm. The metabolite signal estimates from LCModel were fitted to a monoexponential curve as a function of TE's to obtain the T_2 value.

3.2.2.4 Absolute metabolite quantification

For absolute quantification water was used as an internal reference. The metabolite signal estimate at TE = 0 ms was obtained by extrapolation from the monoexponential curve fit. The signal estimate for water at TE = 0 ms was obtained similarly as for metabolite. From the zero-TE signal estimates of metabolites and water, the metabolite concentrations were obtained using an equation

$$C_m = C_w * \left[\frac{LCM_m}{\left(1-e^{\frac{-TR}{T_{1m}}}\right)} \Big/ \frac{LCM_w}{\left(1-e^{\frac{-TR}{T_{1w}}}\right)} \right] \quad [3\text{-}1]$$

where C_m is the metabolite concentration (mM), LCM_m is the LCModel signal estimate for metabolite at TE = 0 ms, LCM_w is the LCModel signal estimate for water at TE = 0 ms, TR is the repetition time and C_w is the water concentration (42 M) [31, 39].

Published T_1 values (1.4 s for tNAA, 1.35 s for tCr, 1.2 s for tCho and 1.5 s for water and lactate) were used to correct for the steady-state T_1 saturation effects (TR = 2 s) [40-42].

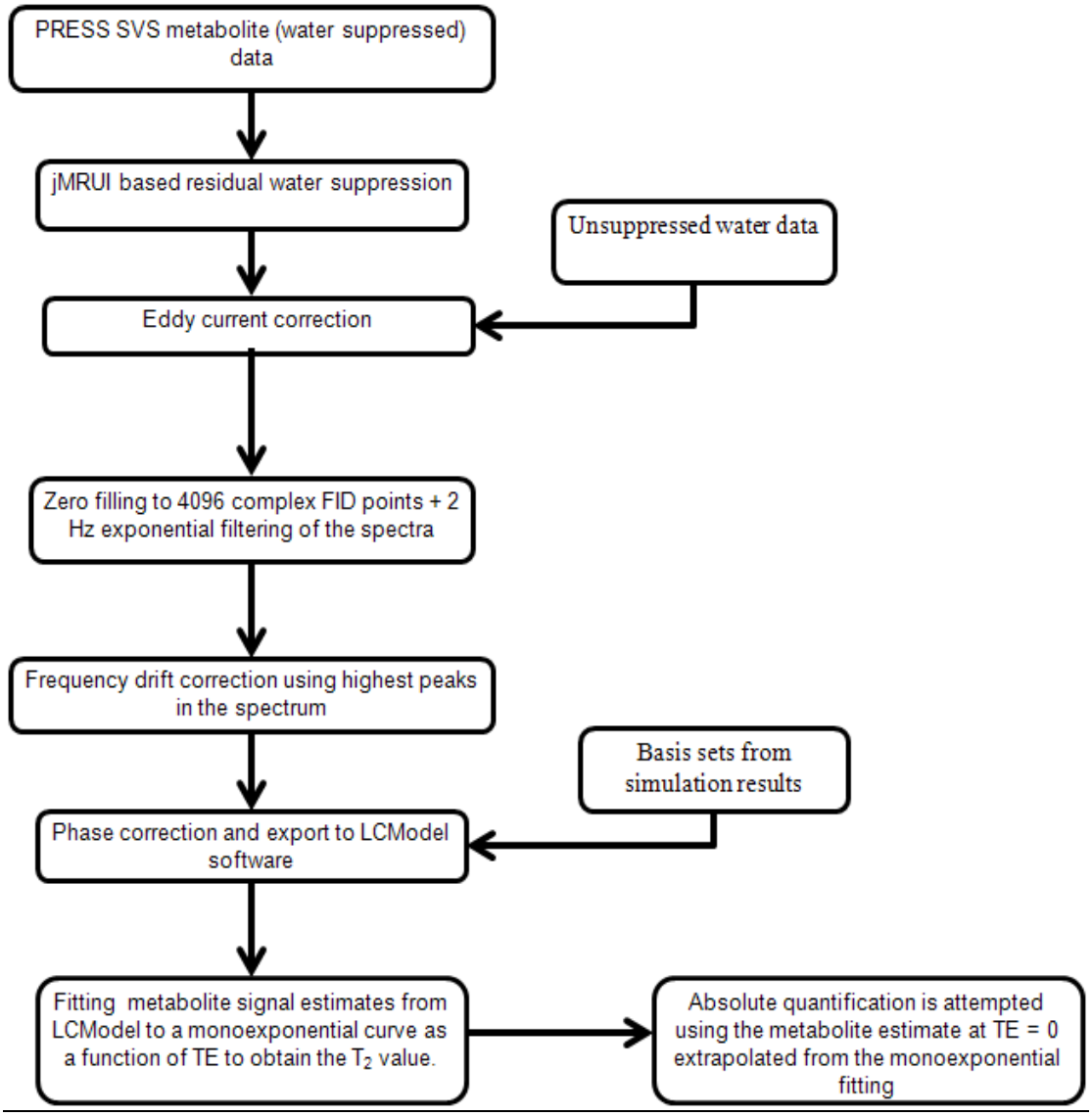

Figure 3-3 Flowchart for the post-processing steps in Data Analysis.

3.2.3 Statistical Analysis

One-way ANOVA analysis was performed to assess difference in T_2 and concentrations among groups. Unpaired t-test was conducted to obtain p values between normal brain and low grade, between normal brain and high grade, and between low grade and high grade. Statistical significance was declared for p-value < 0.05. Bonferroni correction was done by multiplying the p value by the number of metabolites (i.e., 3 excluding lactate). All statistical analyses were conducted using Microsoft Excel (2007) software.

Chapter 4

Results

4.1 Phantom Experiments

Figure 4-1 shows the phantom data acquired from the GE ‘‘Braino’’ phantom at 8 chosen echo times. The signal strength of NAA, Cr and Cho reduced with increasing echo times due to T_2 relaxation whereas for lactate the signal strength as well as the spectral pattern varied with echo times due to the T_2 signal decay and the J coupling effects. The phantom spectra were well reproduced by LCModel fit at all TE’s. The residuals were very small, showing excellent agreement between the phantom and calculated spectra. Figure 4-2 shows the monoexponential fitting of LCModel signal estimates vs. TE for NAA, Cr, Cho and lactate. The monoexponential function used for the fitting was,

$$S = S_0 * \exp(-TE/T_2) \qquad [4\text{-}1]$$

where S denotes the signal estimates at the multiple TEs, S_0 is the signal strength at the zero TE and T_2 is the transverse relaxation. The T_2’s of NAA, Cr, Cho and lactate were calculated as 526 ms, 271 ms, 196 ms and 305 ms respectively. The coefficients of determination (R^2) were all close to unity.

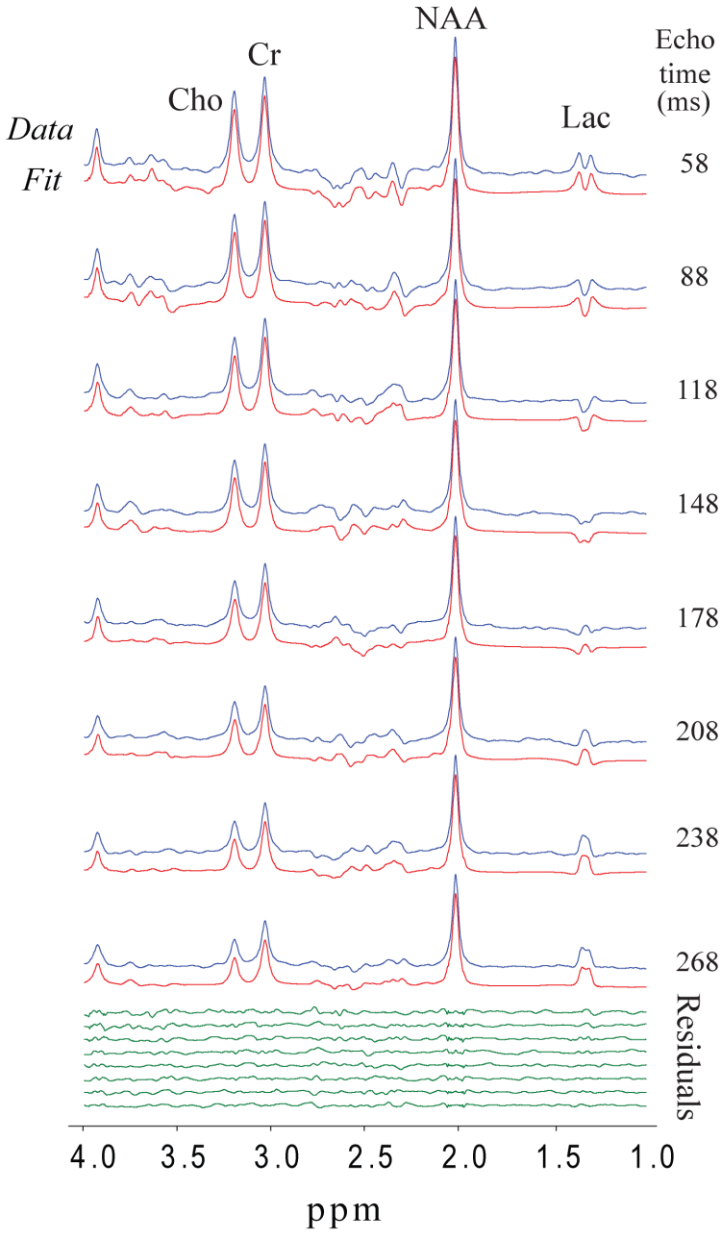

Figure 4-1 Data (blue), LCModel fits (red), and residuals (green) for the GE Braino phantom acquired using PRESS at TE = 58, 88, 118, 148, 178, 208, 238 and 268 ms. Spectra were broadened to a singlet linewidth (FWHM) of 4Hz.

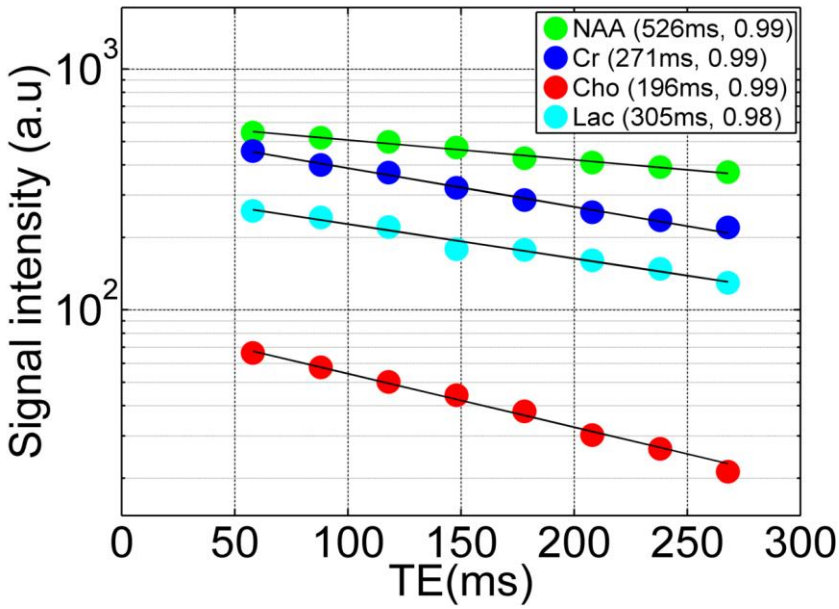

Figure 4-2 Monoexponential fitting of LCModel signal estimates vs. TE for NAA, Cr, Cho and Lac for the GE Braino phantom spectra from Figure 4-1. The T_2 values and the coefficient of determination (R^2) are shown in the legend.

4.2 *In Vivo* Experiments

4.2.1 Normal Brain: Gray matter and white matter regions

In vivo experiments were performed on healthy volunteers. Figure 4-3 shows representative *in vivo* PRESS spectra from the medial occipital and right parietal cortex regions at 8 echo times together with the LCModel fits and residuals. The signal intensity of tCho was quite different between the two voxels which was most likely due to the difference in the gray matter (GM) and white matter (WM) contents within the voxels. Segmentation of the T_1 weighted images showed fractions of GM, WM and CSF as 0.6, 0.2, 0.2 for medial occipital and 0.2, 0.7, 0.1 for right parietal regions respectively. The spectra were reproduced well by the fits and the residuals were at the noise levels. The signal to noise ratio (SNR) for the first echo time was 75 and decreased to 30 at the longest echo time (268 ms). Figure 4-4 shows the monoexponential fits for T_2 estimation

of tNAA, tCr and tCho for the two voxels. The T_2 of tNAA, tCr and tCho for the medial occipital region were 246 ms, 144 ms and 254 ms, respectively, whereas, for the right parietal cortex region they were 310 ms, 156 ms and 234 ms respectively. The mean T_2 of tNAA for the medial occipital region was 260 ± 22 (N = 10) and for the right parietal cortex region was 309 ± 41 (N = 11). The tCr T_2 was 150 ± 7 (N = 10) for the medial occipital region and 151 ± 13 (N = 11) for the right parietal cortex region, and the tCho T_2 was 268 ± 35 (N = 10) for the medial occipital region and 241 ± 8 (N = 11) for the right parietal cortex region. A two tailed unpaired t-test was performed to determine the significance of the differences between the estimated T_2 values in the two regions. The T_2 of tNAA and tCho were significantly different ($p < 0.003$ & $p < 0.02$ but bonferroni corrected $p < 0.06$ respectively) between the two regions, as shown in Figure 4-5.

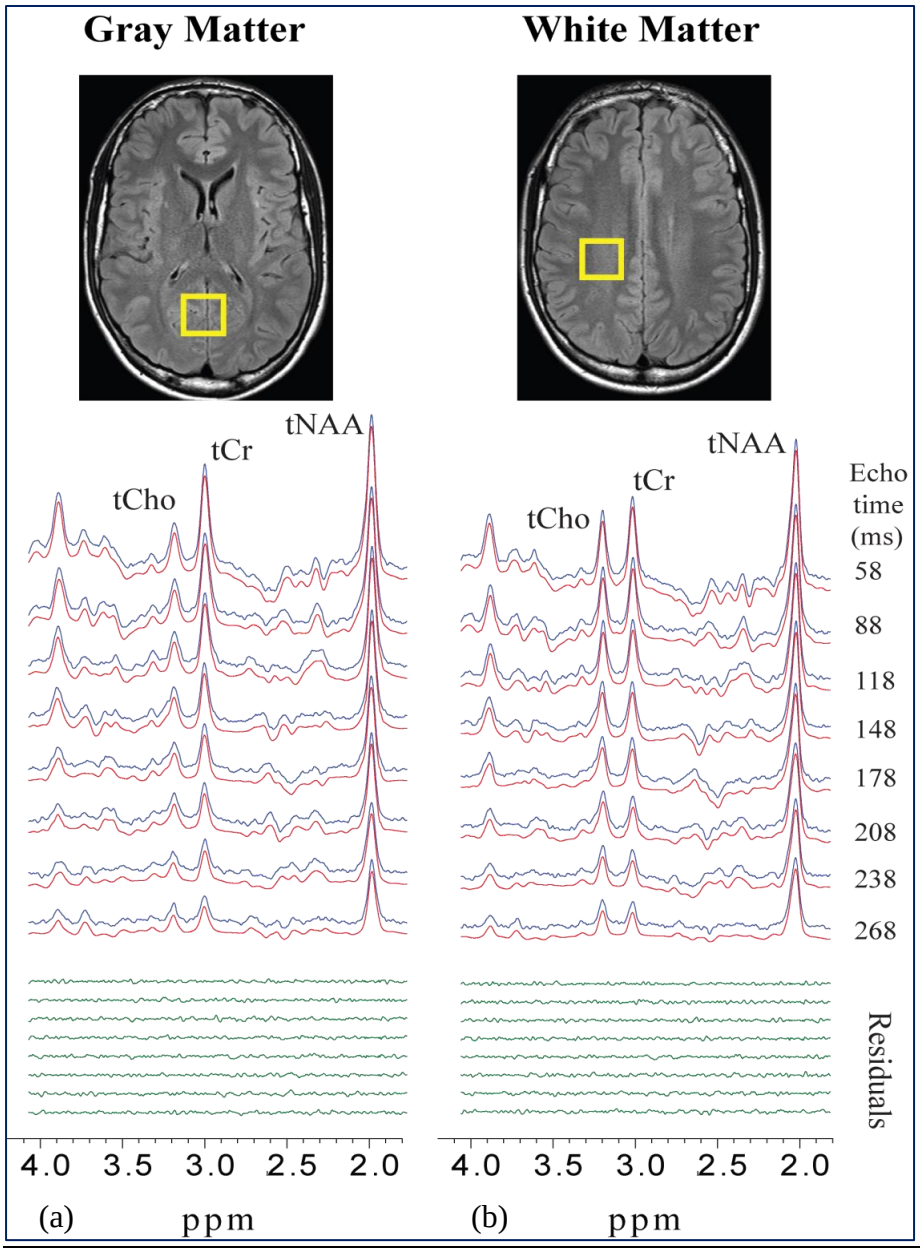

Figure 4-3 *In vivo* spectra (blue), LCModel fits (red) and residuals (green) acquired using PRESS at TE = 58, 88, 118, 148, 178, 208, 238, 268 ms from (a) the medial occipital cortex region and (b) the right parietal cortex region of a healthy volunteer.

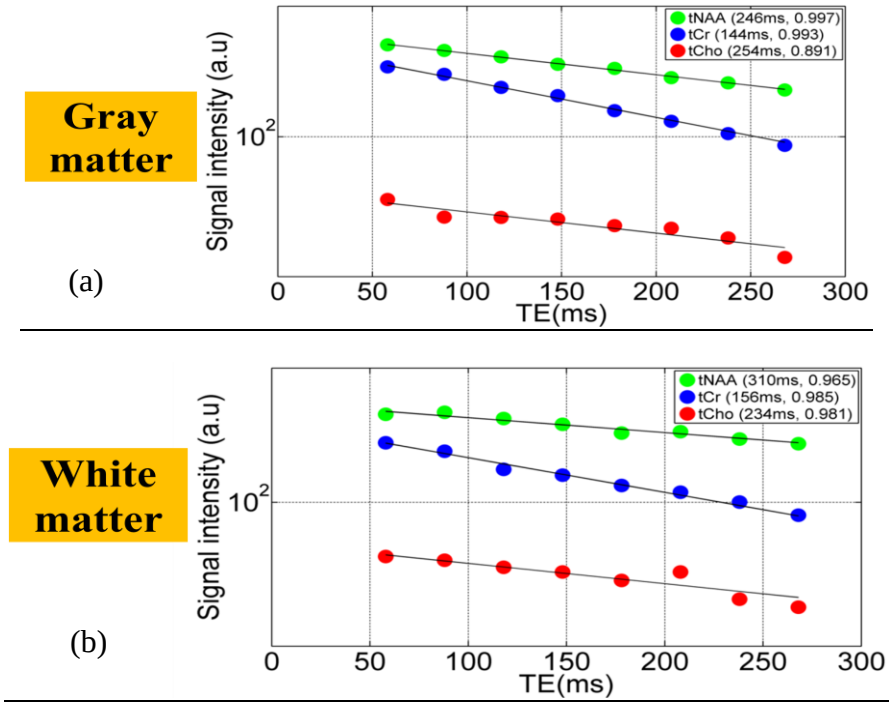

Figure 4-4 Monoexponential fitting of LCModel estimates from the spectra in Figure 4-3 vs. TE for tNAA, tCr and tCho for (a) the medial occipital cortex region and (b) the right parietal cortex region. The T_2 values and the coefficient of determination (R^2) are shown in the legend.

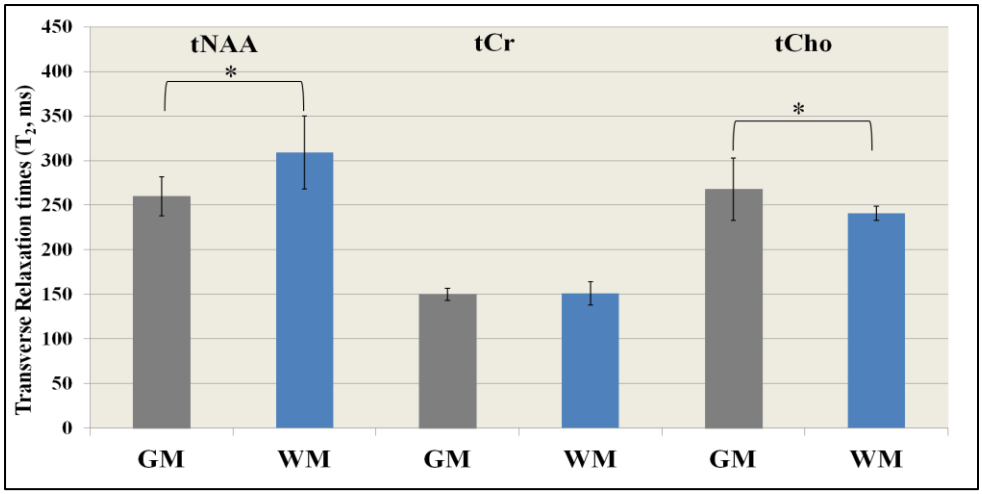

Figure 4-5 Relaxation times (T_2) of tNAA, tCr and tCho for the medial occipital and right parietal cortex regions. An asterisk represents $p < 0.05$. Error bars depict the standard deviation.

4.2.2 Comparison between Tumor and contra-lateral normal brain region

Experiments were performed on tumor patients to compare the T_2 values between tumor and normal appearing contra-lateral brain. Figure 4-6 shows representative *in vivo* spectra with LCModel fits and residuals acquired from the tumor region and from the normal appearing contra-lateral brain region of a low grade tumor patient. The spectra obtained from the tumor show elevated tCho and reduced tCr and tNAA which is characteristic of tumors [41]. The spectra from both regions were reproduced well by the LCModel fits. The residuals did not show substantial variations across the spectral range between 1.8 and 4.1 ppm. Figure 4-7 shows the monoexponential fittings for tNAA, tCr and tCho for the spectra in Figure 4-6. The T_2's of tNAA, tCr and tCho for the tumor location were 234 ms, 158 ms and 308 ms, respectively, whereas, for the contra-lateral normal brain location the values were 235 ms, 148 ms and 237 ms respectively. The metabolite signal decay with increasing TE was well represented by monoexponential fits, giving coefficients of determination (R^2) close to unity. The mean estimated T_2 values (mean ± SD) for the tumor location in the 9 low grade tumor patients were tNAA = 295 ± 33 ms (mean R^2 = 0.89), tCr = 171 ± 19 ms (mean R^2 = 0.98), tCho 297 ± 50 ms (mean R^2 = 0.91) and water 135 ± 18 ms (mean R^2 = 0.99). In contra-lateral normal brain regions the estimated T_2 values were 294 ± 36 ms for tNAA (mean R^2 = 0.95), 152 ± 13 ms for tCr (mean R^2 = 0.97), 244 ± 22 ms for tCho (mean R^2 = 0.93) and 81 ± 7 ms for water (mean R^2 = 0.99) . Figure 4-8 shows that the T_2 of tCr, tCho and water were significantly different between tumor and normal brain ($p = 0.03$ but 0.09 with bonferroni correction, 0.015 and < 0.0001, respectively), however tNAA showed no significant difference ($p = 0.97$) between the regions.

Figure 4-10 shows the comparison of the mean estimated concentrations of tNAA, tCr and tCho between the tumor and contra-lateral normal brain region in the 9 low

grade tumor patients. The estimated concentration in tumors was (mean ± SD) 3.7 ± 1.3 mM for tNAA, 5.71 ± 1.3 mM for tCr and 2.01± 0.5 mM for tCho whereas in the contra-lateral normal brain region the concentration was 8.14 ± 1.4 mM for tNAA, 6.04 ± 1.5 mM for tCr and 1.5 ± 0.2 mM for tCho. The concentrations of tNAA and tCho were significantly different ($p < 0.0001$ & $p < 0.03$ but bonferroni corrected $p < 0.09$ respectively) between tumor and normal brain region as show in Figure 4-10.

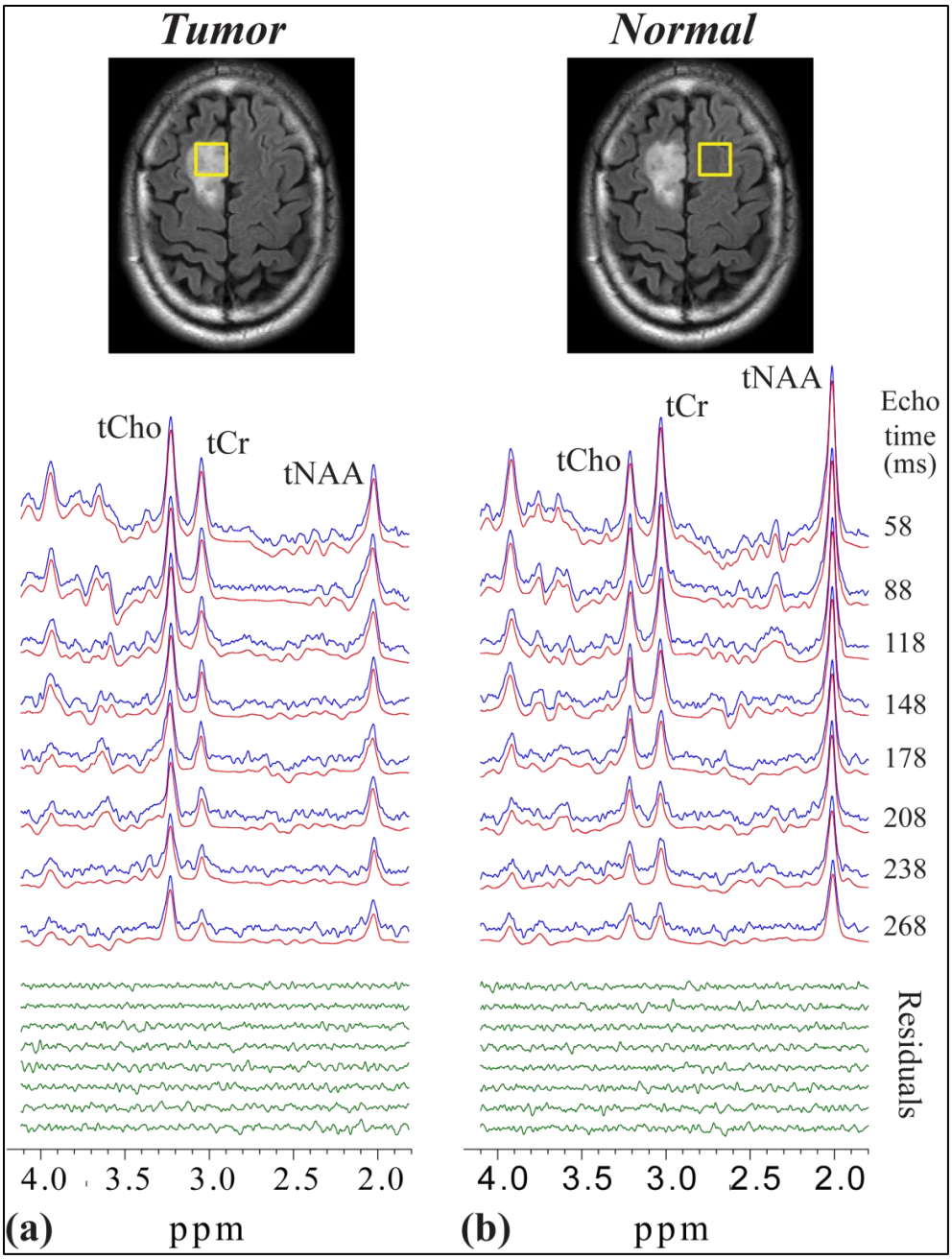

Figure 4-6 *In vivo* spectra (blue), LCModel fits (red) and residuals (green) acquired using PRESS at TE = 58, 88, 118, 148, 178, 208, 238, 268 ms from (a) a FLAIR enhancing region (tumor) and (b) the contra-lateral normal brain region of a tumor patient.

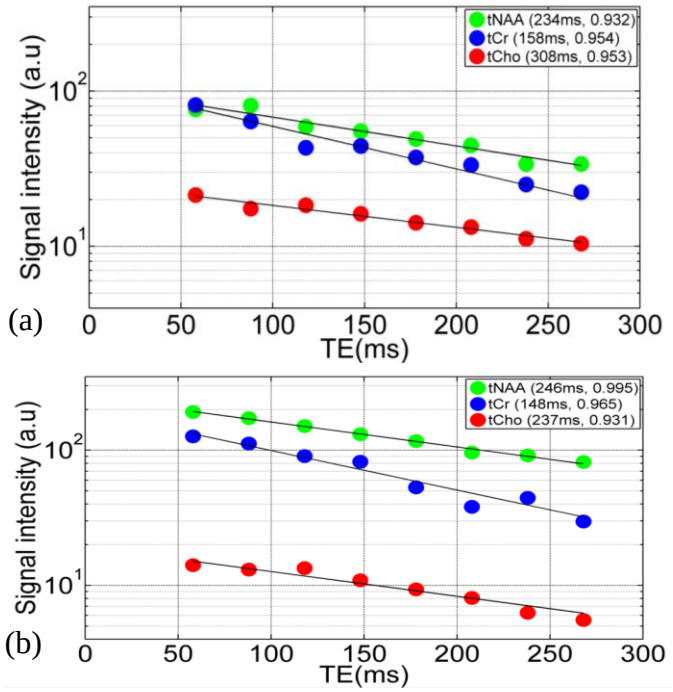

Figure 4-7 Monoexponential fitting of LCModel estimates from the spectra in Figure 4-6 vs. TE for tNAA, tCr and tCho for (a) tumor and (b) contra-lateral normal brain region. The T_2 values and the coefficient of determination (R^2) are shown in the legend.

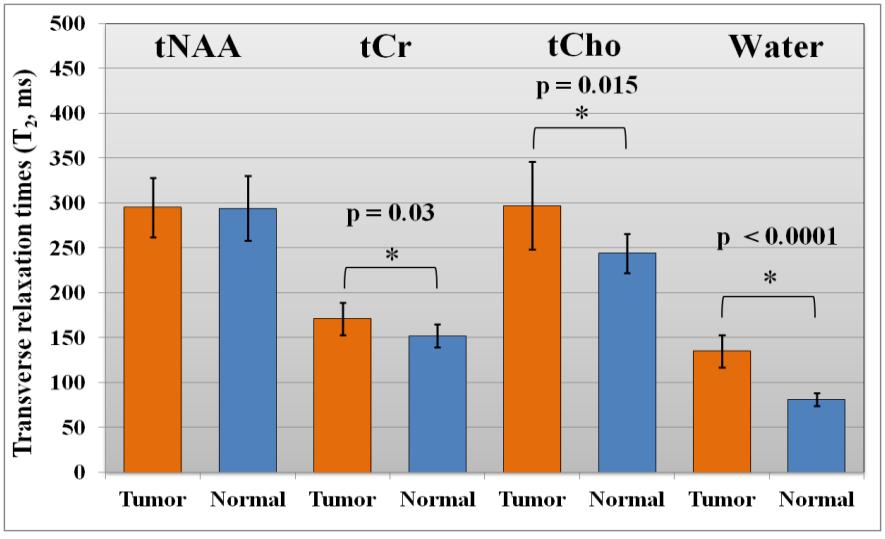

Figure 4-8 Relaxation times (T_2) of tNAA, tCr, tCho and water from tumor and contra-lateral normal brain regions in nine subjects with tumors. tCr, tCho and water show significant difference in T_2 estimates. Error bars depict the standard deviation.

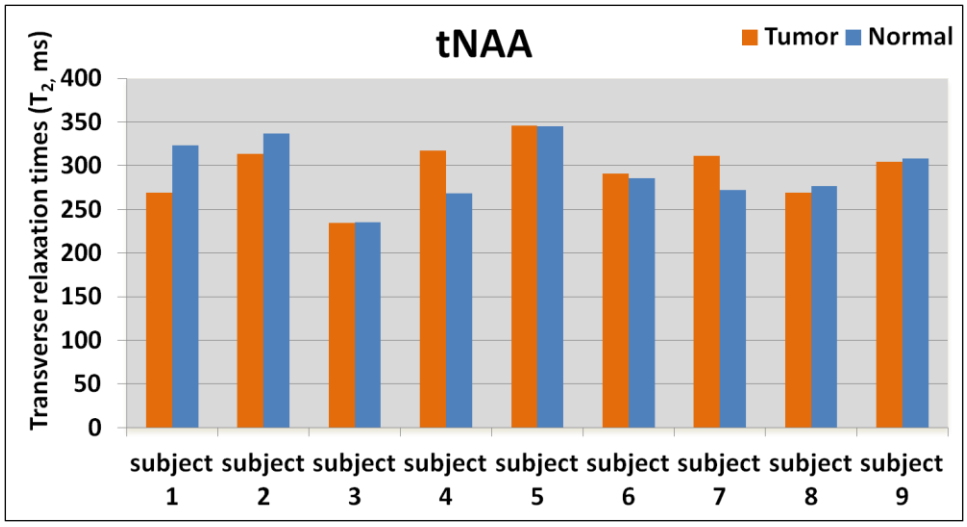

Figure 4-9 Comparison of tNAA relaxation time (T_2) between tumor and contra-lateral normal brain region within the same brain in each of the nine low grade tumor subjects.

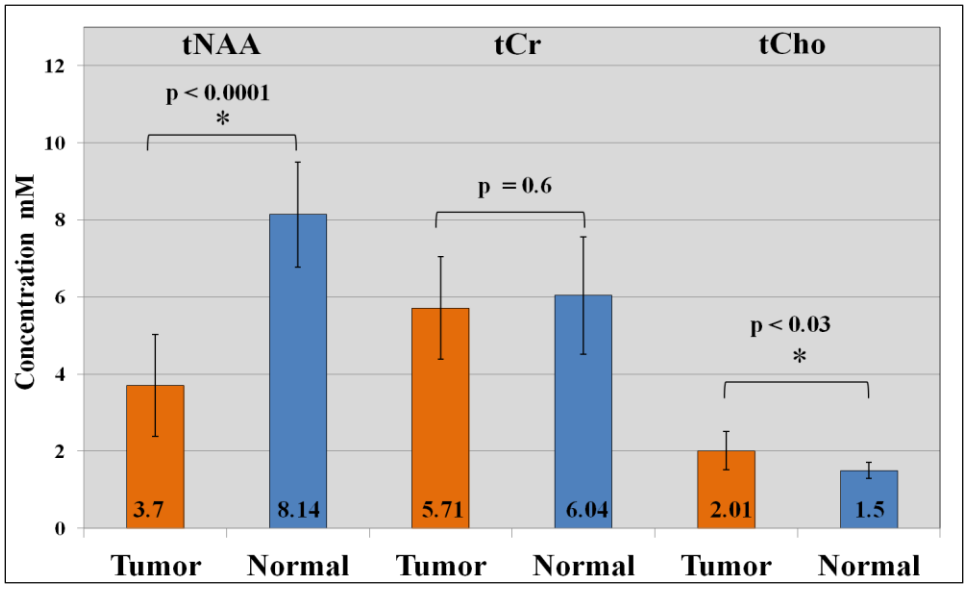

Figure 4-10 Concentrations of tNAA, tCr and tCho in tumor and contra-lateral normal brain regions in nine subjects with tumors. tNAA and tCho show significant difference in concentrations. Error bars depict the standard deviation.

4.2.3 Comparison between Low grade tumor and High grade tumors

Experiments were performed on patients to compare the T_2 values between low grade and high grade tumors. Figure 4-11 shows representative *in vivo* spectra with LCModel fits and residuals acquired from a patient with a low grade tumor and a patient with a high grade tumor. The T_2 for tNAA was not estimated for the low grade tumor spectra as the tNAA signal was very low. The low grade spectra showed a large signal from the lactate resonance at 1.3 ppm. The lactate T_2 was estimated to be 258 ms. The tCr and tCho T_2's for low grade were estimated to be 164 ms and 267 ms respectively. For the high grade tumor spectra the tNAA, tCr and tCho T_2's were estimated to be 230 ms, 172 ms and 288 ms respectively. The lactate in the high grade tumor was too low to measure the T_2.

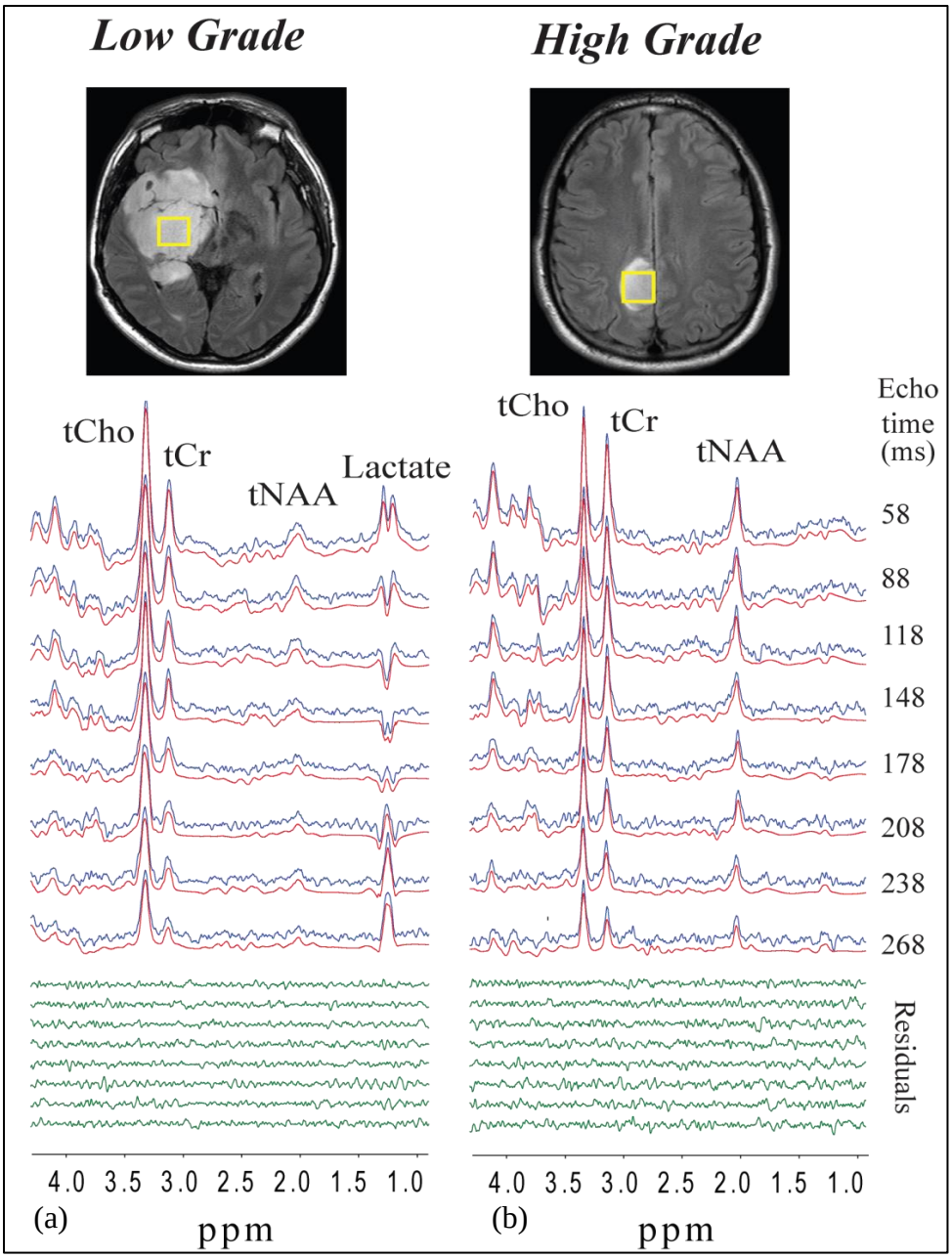

Figure 4-11 *In vivo* spectra (blue), LCModel fits (red) and residuals (green) acquired using PRESS at TE = 58, 88, 118, 148, 178, 208, 238, 268 ms from (a) a low grade tumor patient and (b) a high grade tumor patient.

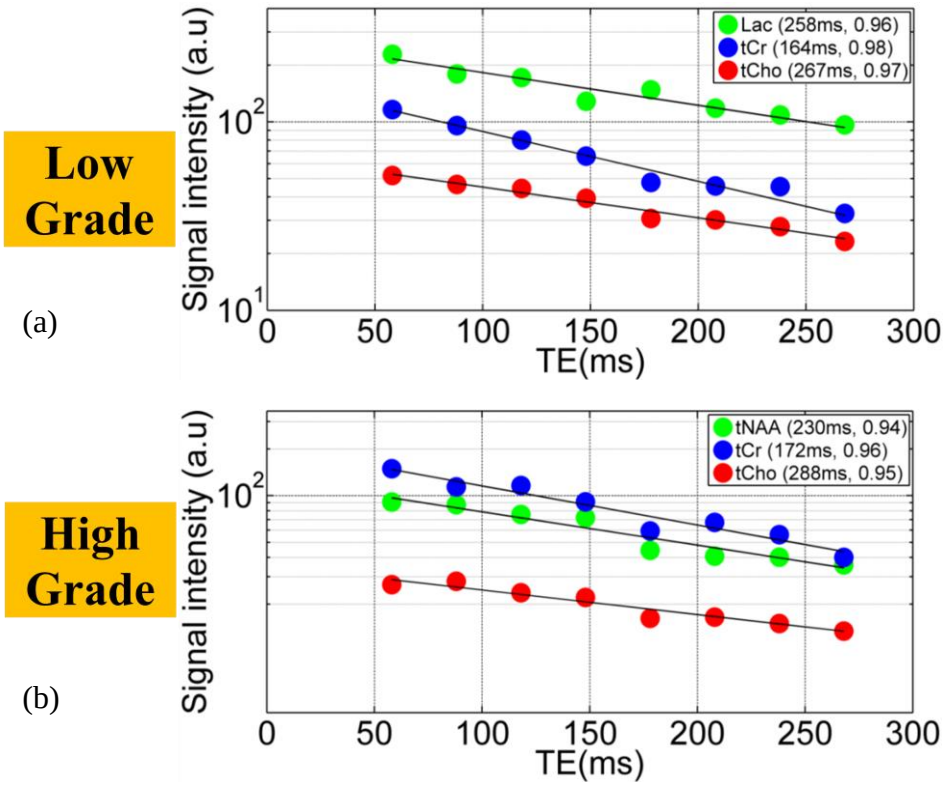

Figure 4-12 Monoexponential fitting of LCModel estimates from the spectra in Figure 4-11 vs. TE for tNAA, tCr and tCho for (a) low grade tumor and (b) high grade tumor. The T_2 values and the coefficient of determination (R^2) are shown in the legend.

4.2.4 Metabolite T_2 comparison between normal brain, low grade, and high grade tumors

Figure 4-13 shows bar graphs for comparison of mean T_2 for tCr between normal brain, low grade and high grade tumors which were estimated to be 149 ± 8 ms (N = 20, mean R^2 = 0.98), 165 ± 22 ms (N = 18, mean R^2 = 0.98) and 180 ± 32 ms (N = 13, mean R^2 = 0.95) respectively. One way ANOVA was performed to assess whether there is a difference in T_2 ($p < 0.0002$) and concentrations ($p < 0.002$) of tCr between normal brain, low grade and high grade tumors. The tCr T_2 was significantly different between normal

brain and low grade tumors ($p < 0.002$), as well as between normal brain and high grade tumors ($p < 0.0001$).

Figure 4-14 shows the comparison of the mean estimated concentrations of tCr between normal brain, low grade and high grade tumors which were estimated to be 7.02 ± 2 mM, 5.14 ± 1.32 mM and 4.52 ± 1.55 mM respectively. The concentration of tCr was significantly different between normal brain and low grade tumor ($p < 0.001$), as well as between normal brain and high grade tumors ($p < 0.01$).

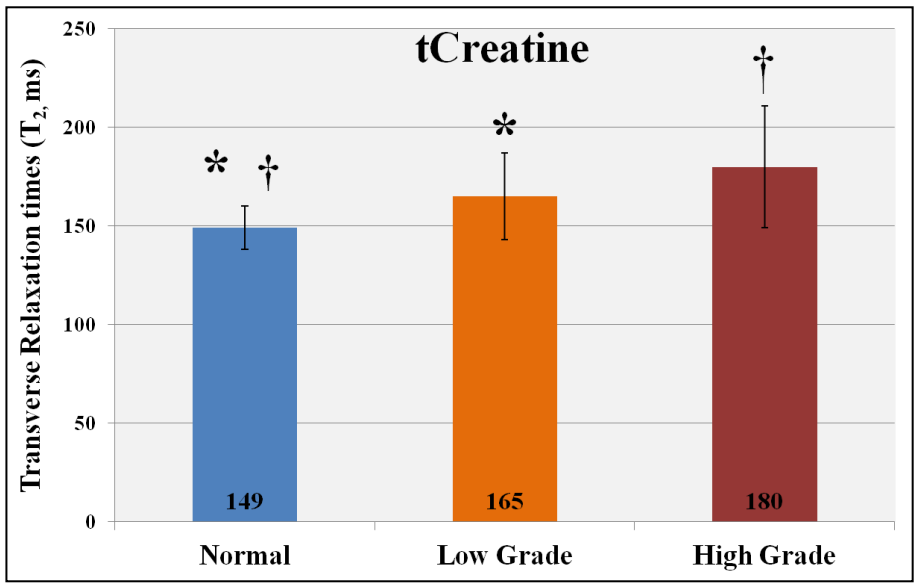

Figure 4-13 Comparison of the tCr T_2 between normal brain, low grade tumors and high grade tumors. Error bars depict the standard deviation.

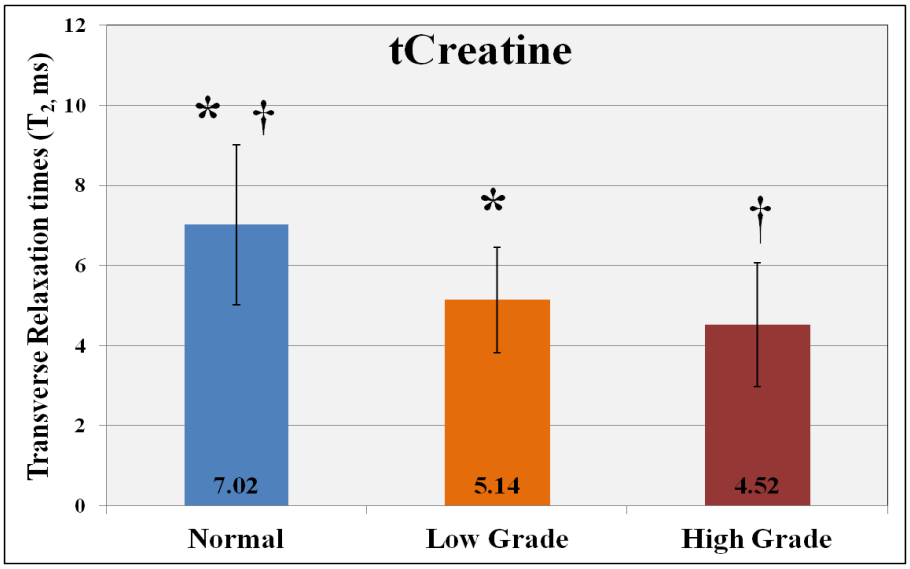

Figure 4-14 Comparison of the concentrations of tCr between normal brain, low grade tumors and high grade tumors. Error bars depict standard deviations.

Similarly Figure 4-15 shows bar graphs for comparison of mean T_2 for tCho which were estimated to be 255 ± 29 ms (N = 21, mean R^2 = 0.92), 291 ± 32 ms (N = 17, mean R^2 = 0.93) and 305 ± 58 ms (N = 15, mean R^2 = 0.92) for normal brain, low grade and high grade tumors respectively. One way ANOVA was performed to assess whether there is a difference in T_2 ($p < 0.001$) and concentrations ($p < 0.001$) of tCho between normal brain, low grade and high grade tumors. The tCho T_2 was significantly different between normal brain and low grade tumors ($p < 0.0008$) as well as between normal brain and high grade tumors ($p < 0.001$).

Figure 4-16 shows the comparison of the mean estimated concentrations of tCho between normal brain, low grade and high grade tumors which were estimated to be 1.32 ± 0.4 mM, 2.1 ± 0.8 mM and 2.5 ± 1 mM respectively. The concentration of tCho was significantly different between normal brain and low grade tumor ($p < 0.001$), as well as between normal brain and high grade tumors ($p < 0.0005$).

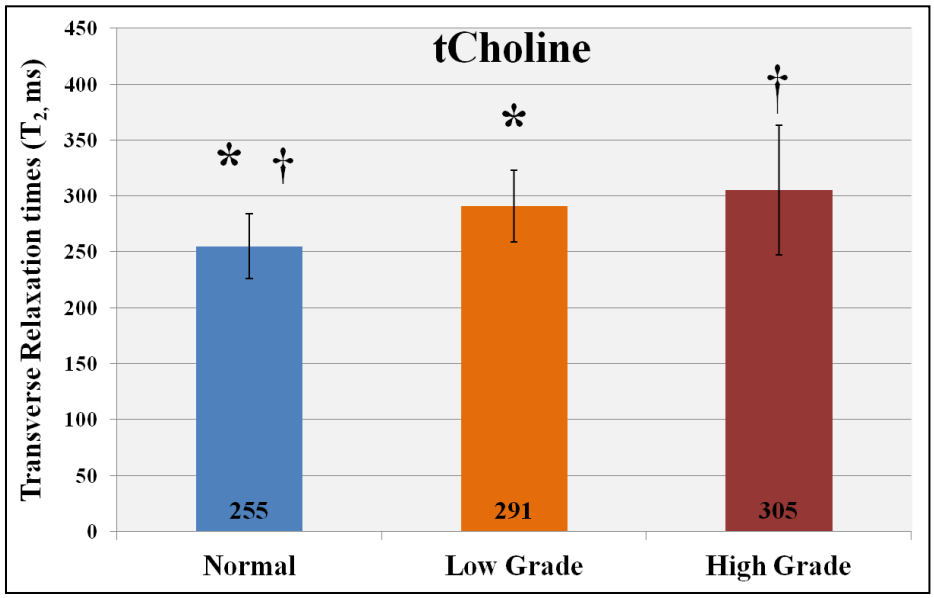

Figure 4-15 Comparison of the tCho T_2 between normal brain, low grade tumors and high grade tumors. Error bars depict standard deviations.

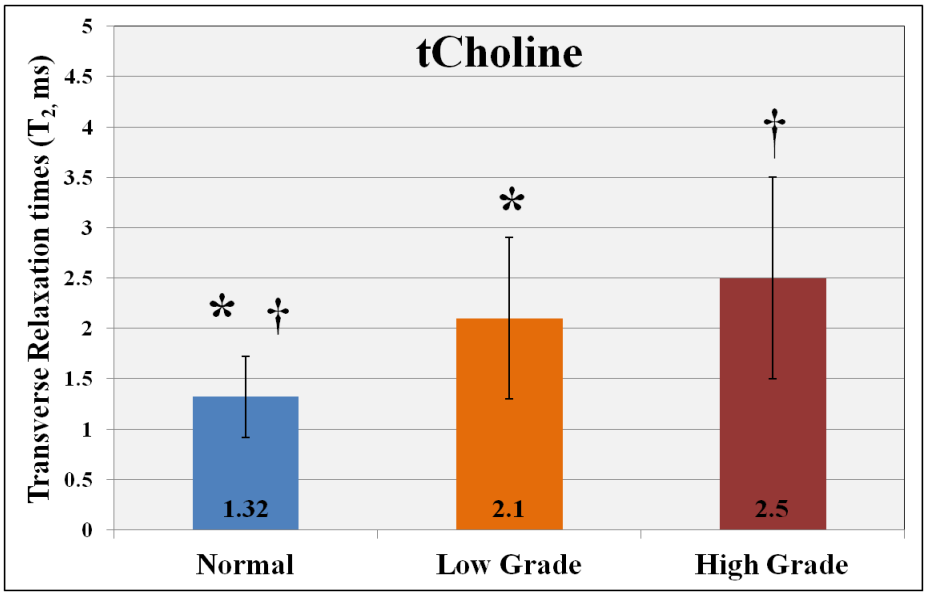

Figure 4-16 Comparison of the concentrations of tCho between normal brain, low grade tumors and high grade tumors. Error bars depict standard deviations.

For the tNAA T_2 comparison between tumor and normal brain, the normal brain data were grouped by gray matter and white matter regions since the NAA T_2 is significantly different between the two regions [40, 42, 43]. Figure 4-18 shows comparison of mean T_2 for tNAA between normal brain white matter, normal brain gray matter, low grade and high grade tumors which were estimated to be 309 ± 41 ms (N = 11, mean R^2 = 0.95), 260 ± 22 ms (N = 10, mean R^2 = 0.96), 276 ± 33 ms (N = 15, mean R^2 = 0.95) and 247 ± 28 ms (N = 13, mean R^2 = 0.91) respectively. One way ANOVA was performed to assess whether there is a difference in T_2 ($p < 0.001$) and concentrations ($p < 10^{-12}$) of tNAA between normal brain, low grade and high grade tumors. The tNAA T_2 was significantly different between normal brain white matter and low grade tumors ($p < 0.02$ but $p < 0.06$ with bonferroni correction), normal brain white matter and high grade tumors ($p < 0.0002$) and between low grade and high grade tumors ($p < 0.02$ but $p < 0.06$ with bonferroni correction).

Figure 4-19 shows the comparison of the mean estimated concentrations of tNAA between normal brain, low grade and high grade tumors which were estimated to be 8.5 ± 1.7 mM, 3.7 ± 1.1 mM and 2.82 ± 1.35 mM respectively. The concentration of tNAA was significantly different between normal brain and low grade tumor ($p < 0.00001$), as well as between normal brain and high grade tumors ($p < 0.00001$).

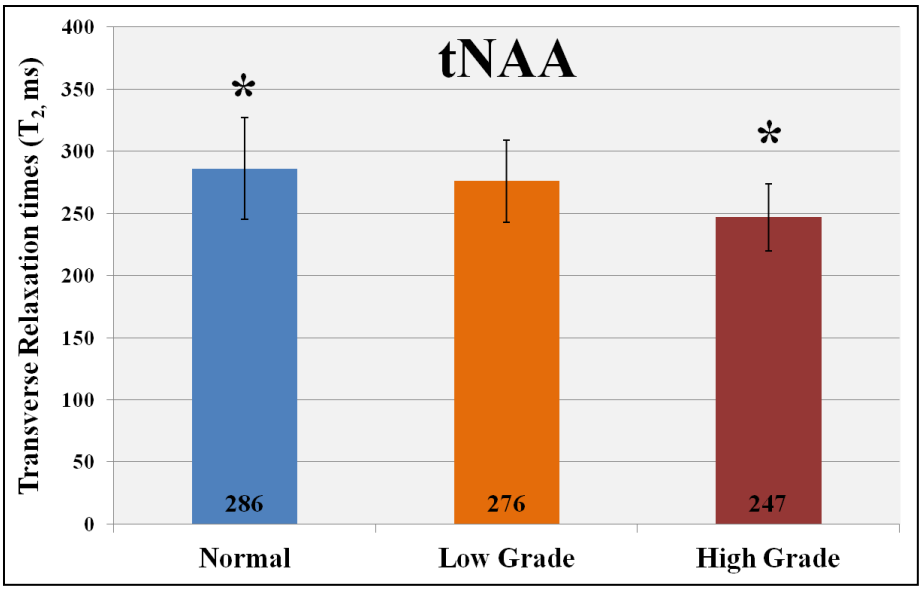

Figure 4-17 Comparison of the tNAA T_2 between normal brain, low grade tumors and high grade tumors. Error bars depict standard deviations.

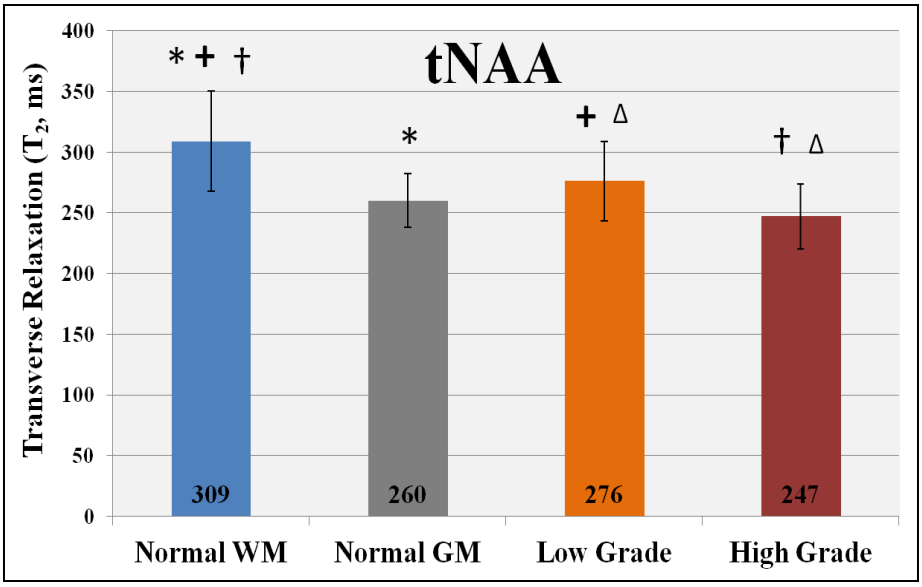

Figure 4-18 Comparison of the tNAA T_2 between normal brain white matter, normal brain gray matter, low grade tumors and high grade tumors. Error bars depict standard deviations.

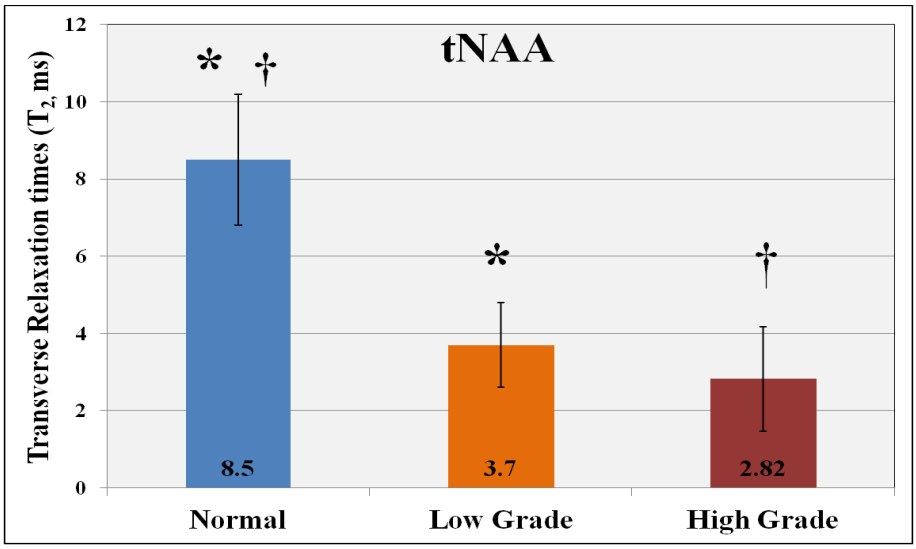

Figure 4-19 Comparison of the concentrations of tNAA between normal brain, low grade tumors and high grade tumors. Error bars depict standard deviations.

4.2.5 Measurement of lactate T_2

The T_2 for lactate was measured in patients when the lactate signal at 1.3ppm was sufficiently large and the lipid and macromolecule (MM) signals at 0.9ppm were not discernible. In these cases, since the lipid signal at 1.3 ppm is not much greater than that at 0.9 ppm in brain tumors (as indicated in short-TE data) the contamination from lipid and MM resonances (1.3 and 1.4 ppm) to lactate estimation was likely minimal (or negligible). Lactate T_2 measurement was performed for data from 7 patients, 4 with low grade and 3 with high grade tumors. Figure 4-20 shows *in vivo* spectra from a patient with a low grade tumor. The figure shows the data, LCModel fit, and the lactate fit, together with the calculated spectra of lactate without T_2 effects. The spectral pattern of the signal at 1.3 ppm in the *in vivo* data was nearly identical to that of the calculated spectra for all echo times. The signal amplitude in the *in vivo* data were progressively decreased as TE increased. Figure 4-21 shows the monoexponential fitting of the lactate signal estimates obtained from LCModel fitting vs. TE's. The TE dependence of the data

was well represented by a monoexponential function (R^2 = 0.96). Figure 4-22 shows the T_2 values for lactate estimated in the 7 tumor patients. The mean lactate T_2 was 256 ± 22 ms (mean R^2 = 0.93). Figure 4-23 shows the lactate concentration estimated in the 7 tumor patients. The mean concentration was 6.71 ± 2.45 mM in the 7 patients and there was no significant difference between the low grade and high grade tumors ($p > 0.05$).

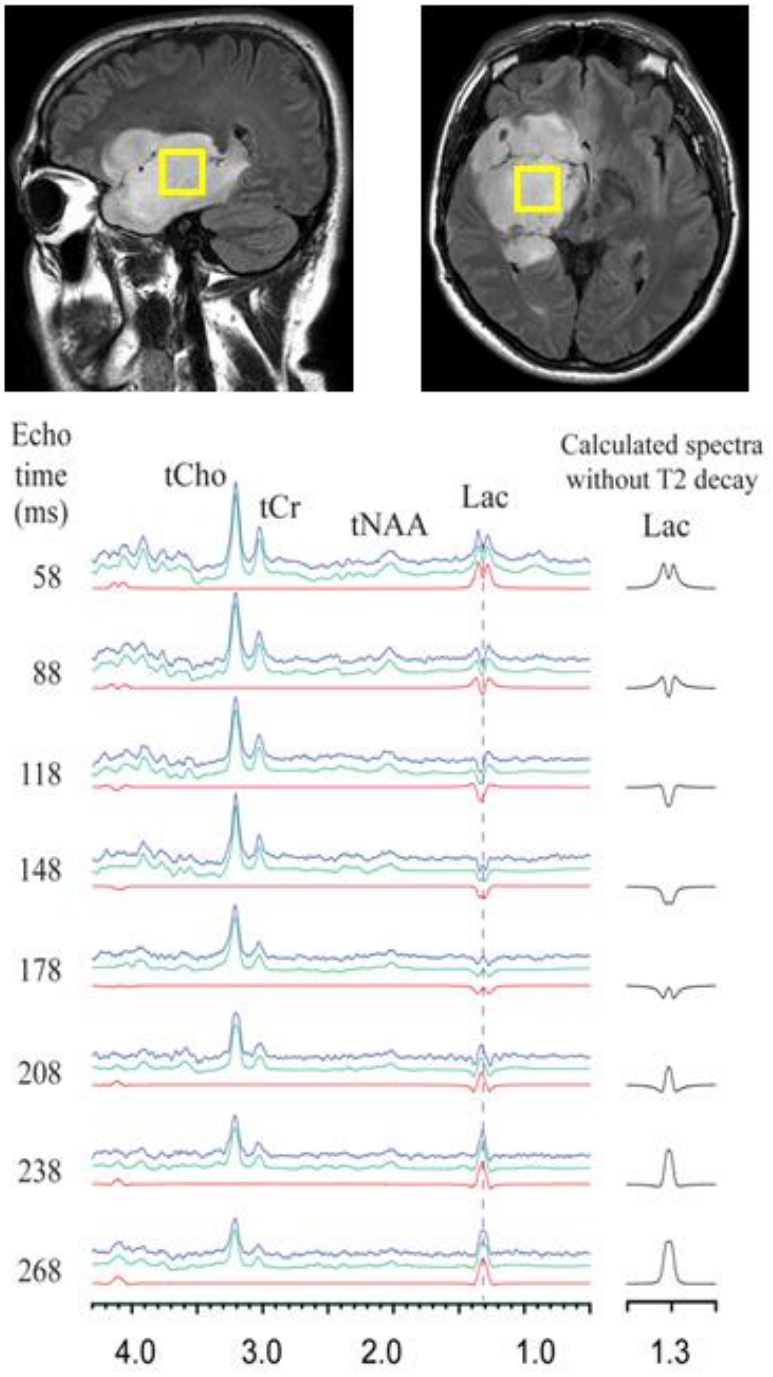

Figure 4-20 Representative *In vivo* spectra (blue), LCModel fits (green) and fit (red) for lactate T_2 estimation. Calculated spectra of lactate without T_2 decay (black) are shown on the right. *In vivo* data were acquired from a voxel positioned within the tumor of a low grade tumor patient, as shown in T2w-FLAIR images.

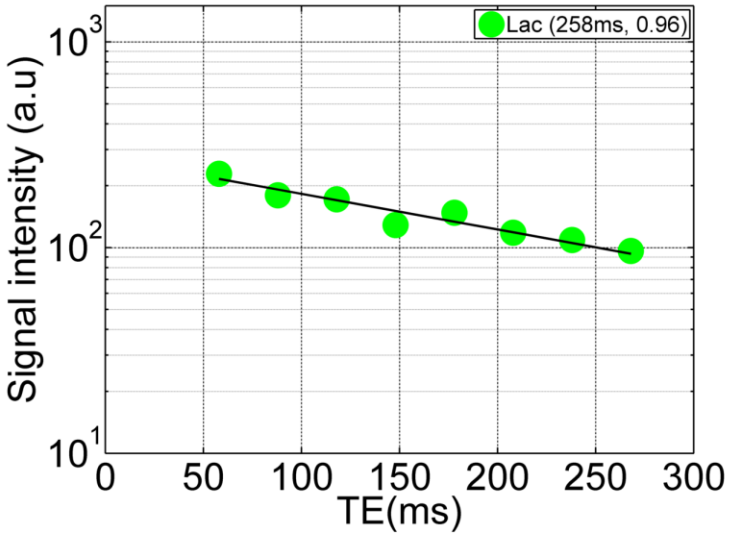

Figure 4-21 Monoexponential fitting of LCModel estimates vs. TE's of lactate for the low grade tumor spectra shown in Figure 4-20. The T_2 value and the coefficient of determination (R^2) are shown in the legend.

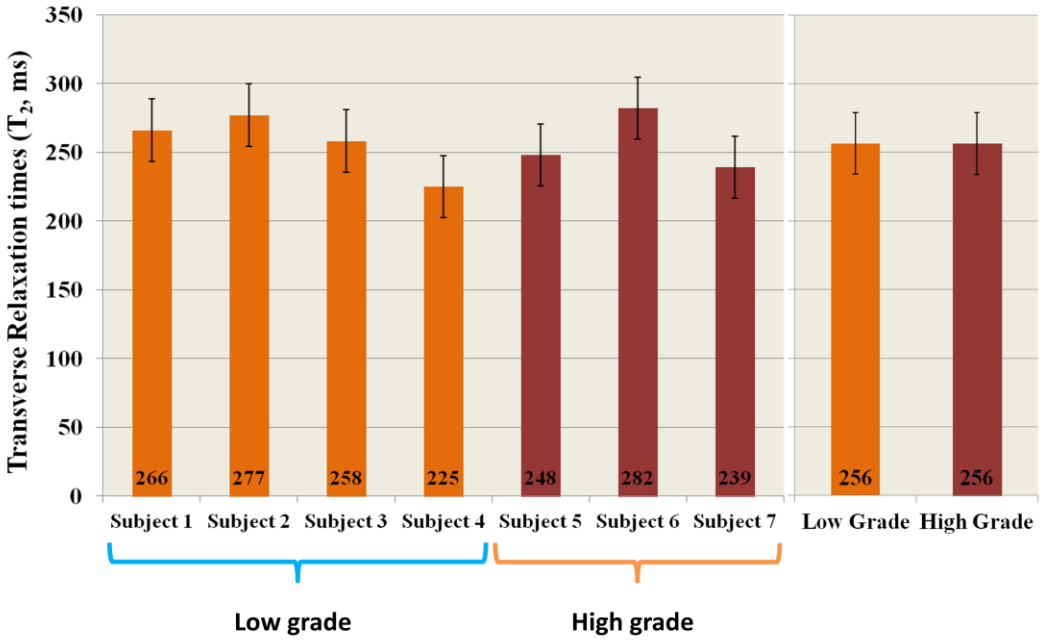

Figure 4-22 Estimated T_2 values for lacate in 4 low grade tumors and 3 high grade tumors. Mean T_2 in low grade tumors and high grade tumors. The error bars depict the standard deviation.

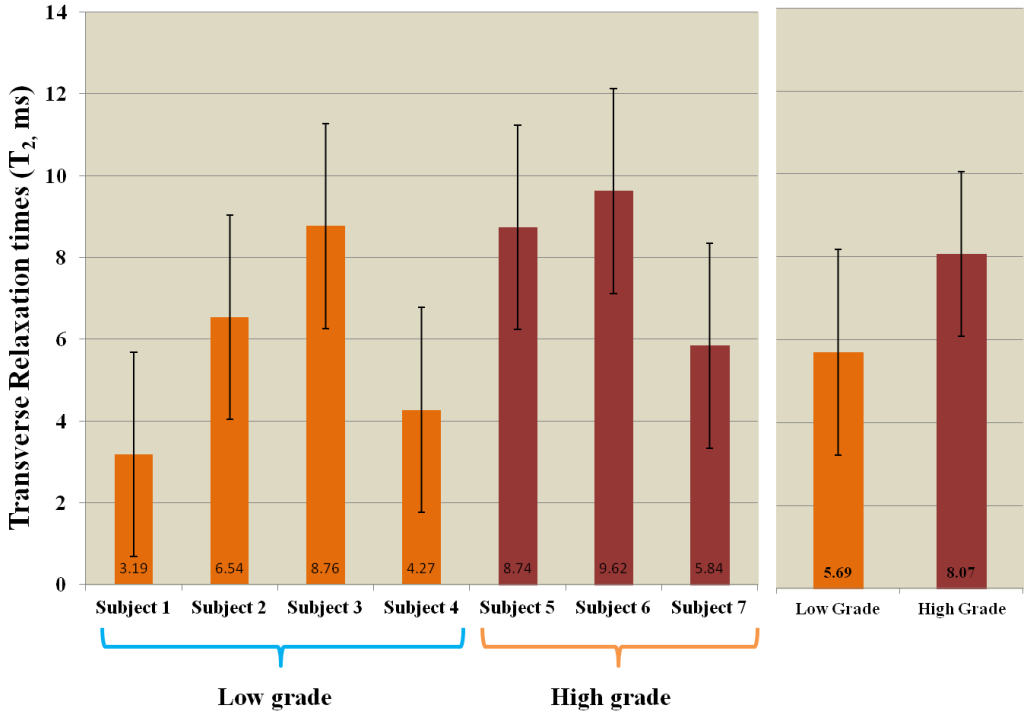

Figure 4-23 Estimated concentrations for lacate in 4 low grade tumors and 3 high grade tumors. The error bars depict the standard deviation.

Chapter 5

Discussion

This study observed that the tNAA T_2 is longer in white matter dominant regions compared to gray matter dominant regions in normal brain. Previous T_2 studies in normal brain by Traber et al [40], Mlynarik et al [42], Ganji et al [43] and Brief et al [44] have reported similar observations. The estimated T_2 of tNAA in medial occipital (260 ms) and right parietal cortex regions (310 ms) in this study are similar to the values published in the aforementioned studies for occipital gray and parietal white matter regions [40, 42-44]. The estimated T_2 of tCr and tCho in gray and white matter dominant regions were also in agreement with previous studies [40, 43].

tNAA T_2 was similar between tumor and contra-lateral normal brain region (Figure 4-9). Data showed a relatively large inter subject variation in tNAA T_2 estimates between patients, likely due to the effects of tumor heterogeneities. The mean tNAA T_2 in normal brain (gray matter and white matter) did not show significant difference when compared with the mean T_2 in low grade tumors. However, a significant difference was present between the tNAA T_2 values between low grade tumors and normal brain white matter. This observation was consistent with the study by Isobe et al [11]. The T_2 for tNAA in high grade tumors was significantly shorter than the T_2 in normal brain white matter as well as in low grade tumors. A similar trend was observed in the study by Isobe et al [11] and Li et al [41]. The tCr and tCho T_2's were significantly longer in tumors than in contra-lateral normal brain, most likely because of alterations in the cellular environment in tumor cells. The changes in cellular environment, which can cause a change in T_2, include, involvement of paramagnetic material [11], changes in intracellular energy metabolism [45], pH [45], oxygen pressure [46], intracellular skeleton as well as structural strain on the intracellular space [11].

Choline containing compounds play a key role in biosynthesis of phosphatidylcholine, other membrane lipids and acetyl choline. The concentration of choline containing compounds is very useful as a marker of cell-membrane synthesis and degradation in glial growth, injury and repair [47, 48]. Both low grade and high grade tumors may have increased cellularity, which require production of choline containing compounds. Previous studies have reported an increase in PC and PC/GPC in tumors [27, 49]. The observation of lengthened T_2 of tCho in tumors may indicate that the mobility of Cho is increased in high-cellularity environments. The longer T_2 of tCr may be explained by the change in metabolic composition due to an increased rate of the breakdown of PCr to Cr. PCr contains a high energy phosphate bond, which transfers to adenosine diphosphate (ADP) when it is broken down to Cr. Reduced PCr has been observed in gliomas which suggests that there is a high energy requirement for maintaining the growth of cells in gliomas [50].

For lactate measurement, many previous studies have used long echo time approaches which allow refocusing of the J-modulation of the CH_3 protons for detection and quantification [51, 52]. Hence, to accurately quantify the concentration of lactate, prior knowledge of its transverse relaxation rate is essential. There are very few studies that reported the transverse relaxation rate of lactate [53-56]. These studies measured the change in the peak amplitude of lactate at a limited number of echo times. Previous studies have reported the T_2 of lactate in conditions like chronic infarction [54, 55], stroke [53] and developing brain [56]. Lactate T_2 measurement in tumors has not been reported to date. The study in chronic infarction patients reported lactate T_2 as 225 ms but only in one patient, whereas Frahm et al [54] reported it as 1200ms. In the study by Blamire et al [53] in stroke patients the lactate T_2 was measured to be 780 ms (mean), with large variations (i.e., 186 - 2110 ms). In all the above studies data was acquired only at 2 echo

times. The disadvantage of using two TE data points is that the quality of the line fit cannot be assessed. In the present study 8 TE data points were used which may have provided improved precision in lactate T_2 estimation. In the present study, the mean T_2 estimate of lactate was 256 ± 22 ms with a mean R^2 value of 0.93.

For absolute quantification of tNAA, tCr and tCho, a short TE (< 30 ms) approach can be used as these metabolite signals are well defined and the T_2 effects at the short TE's are minimal. However, lactate detection in many studies, has been accomplished using long TE (i.e. 144 ms [31, 39]). Quantification at long TE is severely affected by T_2 relaxation effects, hence, to precisely quantify lactate concentration it is essential to correct for T_2 relaxation.

For singlets such as NAA, Cr and Cho the signal intensity is influenced by T_2 relaxation effects only, but for lactate, the signal intensity and the spectral pattern both vary with changing TE due to T_2 relaxation and J coupling effects. In this study, the J evolution effects on the metabolite signals were incorporated into the basis spectra created for spectral fitting, which allowed estimation of the transverse relaxation time from the TE dependence of the spectral fitting estimates. Furthermore, since the basis spectra were calculated using the slice selective RF and gradient pulse parameters used for PRESS data acquisition, the spectral fitting allowed precise signal estimates of metabolites, particularly lactate.

The shortest TE of the present T_2 measurement study was 58 ms, which was the minimum possible TE for the chosen RF pulses and spoiler gradients in the scanner. Thus the method may be valid for metabolite signals whose T_2 is relatively long. Large signals from macromolecules (MM) are present at short TE, complicating the spectral analysis in brain MRS. Since the MM T_2 is ~5 fold shorter than metabolite T_2 [57], the MM signals are markedly reduced at TE = 58 ms and longer, while metabolite signals remain

with acceptable SNR. This T_2 difference between MM and metabolite signals simplifies the metabolite spectra substantially. In addition, it is likely that lipids have shorter T_2 than metabolites [58, 59]. Taken together, the multiple TEs chosen for the present study may be appropriate for estimating metabolite T_2 values without substantial interferences from MM and lipids.

One of the confounding factors in lactate measurement is the slice displacements arising when the bandwidth of the 180° pulse is not much greater than the spectral distance between the lactate 1.3 and 4.1 ppm resonances [60-62]. In this study the 180° pulse had a bandwidth of 1.27 kHz and the RF carrier was set at 2.5 ppm. The slices of lactate CH_3 resonance selected by the 180° pulses were displaced by ~12% with respect to the planned slice which resulted in no signal from a part of the voxel of interest (VOI) and contamination signals from outside the VOI. The slice displacement for the PRESS 90° pulse was small (< 4%) because of the large bandwidth (4.2 kHz) of the RF pulse. Using RF pulses with large bandwidths is important for minimizing the partial volume artifacts and the signal degradation due to chemical shift displacement effects.

Molecular diffusion may occur during an MRS sequence. A molecule in motion can experience different field strengths in time. This diffusion may cause incomplete refocusing and consequently signal reduction in addition to T_2 signal decay. This effect can increase with increasing TE. The signal reduction due to molecular diffusion effects may be increased with the use of spoiler gradient pulses. Prior studies showed that the diffusivity of brain metabolites is as low as 0.3×10^{-9} m^2/s [63-65]. The spoiling gradient pulses used for the present study were much shorter and weaker than those used in the prior MRS diffusion study [63-65]. For spoiling gradients of 4-ms duration, 20 mT/m strength, and center-to-center interval of 17 ms between the spoilers within the PRESS,

the signal loss due to diffusion effects is predicted to be < 0.5% at all TEs, indicating that errors in T_2 estimation due to the diffusion effects may be negligible in the present study.

In this study, a constant TR of 2 s was used for acquisitions at all TE's. Since the TR was not much longer than metabolite T_1 (1.2 – 1.5 s) [40-42], the initial longitudinal magnetization in the steady state condition was smaller than the thermal equilibrium magnetization. For the PRESS sequence used, assuming instantaneous 180° rotations by the 180° RF pulses, the ratio of the steady-state initial longitudinal magnetization to the thermal equilibrium magnetization may be given by

$$\frac{\mathrm{M\,ini}}{\mathrm{M0}} = 1 - \mathrm{E_{TR}} + 2\mathrm{E_{TR}}\mathrm{E_1} - 2\mathrm{E_{TR}}\mathrm{E_2} \qquad [5\text{-}1]$$

where $E_{TR} = \exp(-TR/T_1)$, $E_1 = \exp((TE_1/2)/T_1)$ and $E_2 = \exp((TE_1 + TE_2/2)/T_1)$

Equation 5-1 indicates that the initial longitudinal magnetization is decreased with increasing TE, thereby leading to shortening of T_2. However, errors due to the use of 2 s TR appear to be negligible. Given that the longest published T_1 value of the metabolites of interest is 1.5 s, underestimation of T_2 in the present study is calculated to be less than 3%.

Chapter 6

Conclusion

The purpose of this study was to measure the T_2 relaxation times of major singlets (tNAA, tCr and tCho) and lactate in tumors, to compare the tumor T_2 values with contra-lateral normal brain T_2, and to compare the T_2 values between tumor grades. The results showed a difference in T_2 relaxation times of tCr and tCho and a difference in concentrations of tNAA and tCho between tumor and contra-lateral normal brain. It was also observed that the T_2 relaxation time of tNAA is different between low grade and high grade tumors and between normal brain and high grade tumors. The T_2 relaxation time of lactate in tumors was measured for the first time. With the measured T_2 relaxation time of lactate, estimation of the zero-TE signal for lactate quantification was performed. The T_2 relaxation time and the concentration of lactate did not show significant difference between low grade and high grade tumors.

Further investigation in a larger patient population is required to evaluate the difference in T_2 and concentration of lactate between low grade and high grade tumors. All in all, this study paves the way for future studies to explore the possibility of using metabolite T_2 relaxation as a diagnostic and prognostic marker for brain tumors.

References

1. Rabi, I.I., et al., *A New Method of Measuring Nuclear Magnetic Moment.* Physical Review, 1938. **53**(4): p. 318-318.

2. Castillo, M., L. Kwock, and S.K. Mukherji, *Clinical applications of proton MR spectroscopy.* American Journal of Neuroradiology, 1996. **17**(1): p. 1-15.

3. McKnight, T.R., *Proton magnetic resonance spectroscopic evaluation of brain tumor metabolism.* Seminars in Oncology, 2004. **31**(5): p. 605-617.

4. Ishimaru, H., et al., *Differentiation between high-grade glioma and metastatic brain tumor using single-voxel proton MR spectroscopy.* European Radiology, 2001. **11**(9): p. 1784-1791.

5. Majos, C., et al., *Brain tumor classification by proton MR spectroscopy: Comparison of diagnostic accuracy at short and long TE.* American Journal of Neuroradiology, 2004. **25**(10): p. 1696-1704.

6. Gajewicz, W., et al., *The use of proton MRS in the differential diagnosis of brain tumors and tumor-like processes.* Medical science monitor : international medical journal of experimental and clinical research, 2003. **9**(9): p. MT97-105.

7. Joseph B. Lambert, E.P.M., *Nuclear Magnetic Resonance Spectroscopy: An Introduction to Principles, Applications, and Experimental Methods*2004: Pearson.

8. Graaf, R.D., *in vivo NMR spectroscopy*. 2 ed. Vol. 2. 2008: Wiley.

9. Reich, H.J. *Structure Determination Using Spectroscopic Methods*. 2013; Available from: http://www.chem.wisc.edu/areas/reich/chem605/index.htm.

10. Bloembergen, N., E.M. Purcell, and R.V. Pound, *Relaxation Effects in Nuclear Magnetic Resonance Absorption.* Physical Review, 1948. **73**(7): p. 679-712.

11. Isobe, T., et al., *Quantification of cerebral metabolites in glioma patients with proton MR spectroscopy using T2 relaxation time correction.* Magnetic Resonance Imaging, 2002. **20**(4): p. 343-349.

12. Antonini, A., et al., *T2 Relaxation-Time in Patients with Parkinsons-Disease.* Neurology, 1993. **43**(4): p. 697-700.

13. Chen, J.C., et al., *Mr of Human Postmortem Brain-Tissue - Correlative Study between T2 and Assays of Iron and Ferritin in Parkinson and Huntington Disease.* American Journal of Neuroradiology, 1993. **14**(2): p. 275-281.

14. Du, F., et al., *Water and metabolite transverse T2 relaxation time abnormalities in the white matter in schizophrenia.* Schizophrenia Research, 2012. **137**(1-3): p. 241-245.

15. Ongur, D., et al., *T(2) Relaxation Time Abnormalities in Bipolar Disorder and Schizophrenia.* Magnetic Resonance in Medicine, 2010. **63**(1): p. 1-8.

16. Louis, D.N., et al., *The 2007 WHO classification of tumours of the central nervous system.* Acta Neuropathologica, 2007. **114**(2): p. 97-109.

17. Barker, P.B. and D.D.M. Lin, *In vivo proton MR spectroscopy of the human brain.* Progress in Nuclear Magnetic Resonance Spectroscopy, 2006. **49**(2): p. 99-128.

18. Pouwels, P.J.W. and J. Frahm, *Regional metabolite concentrations in human brain as determined by quantitative localized proton MRS.* Magnetic Resonance in Medicine, 1998. **39**(1): p. 53-60.

19. Vanderknaap, M.S., et al., *Age-Dependent Changes in Localized Proton and Phosphorus Mr Spectroscopy of the Brain.* Radiology, 1990. **176**(2): p. 509-515.

20. Jacobs, M.A., et al., *Quantitative proton MR spectroscopic imaging of normal human cerebellum and brain stem.* Magnetic Resonance in Medicine, 2001. **46**(4): p. 699-705.

21. Saunders, D.E., et al., *Aging of the adult human brain: In vivo quantitation of metabolite content with proton magnetic resonance spectroscopy.* Jmri-Journal of Magnetic Resonance Imaging, 1999. **9**(5): p. 711-716.

22. Howe, F.A., et al., *Metabolic profiles of human brain tumors using quantitative in vivo H-1 magnetic resonance spectroscopy.* Magnetic Resonance in Medicine, 2003. **49**(2): p. 223-232.

23. Tate, A.R., et al., *Automated classification of short echo time in in vivo H-1 brain tumor spectra: A multicenter study.* Magnetic Resonance in Medicine, 2003. **49**(1): p. 29-36.

24. Fulham, M.J., et al., *Mapping of Brain-Tumor Metabolites with Proton Mr Spectroscopic Imaging - Clinical Relevance.* Radiology, 1992. **185**(3): p. 675-686.

25. Stadlbauer, A., et al., *Preoperative grading of gliomas by using metabolite quantification with high-spatial-resolution proton MR spectroscopic imaging.* Radiology, 2006. **238**(3): p. 958-969.

26. Peter B. Barker, A.B., Nicola De Stefano, Rao Gullapalli, Doris D.M. Lin, *Clinical MR Spectroscopy: Techniques and Applications*2009: Cambridge University Press.

27. Podo, F., *Tumour phospholipid metabolism.* Nmr in Biomedicine, 1999. **12**(7): p. 413-439.

28. Pedersen, P.L., *Warburg, me and hexokinase 2: Multiple discoveries of key molecular events underlying one of cancers' most common phenotypes, the "Warburg Effect", i.e., elevated glycolysis in the presence of oxygen.* Journal of Bioenergetics and Biomembranes, 2007. **39**(3): p. 211-222.

29. Kugel, H., et al., *Human Brain-Tumors - Spectral Patterns Detected with Localized H-1 Mr Spectroscopy.* Radiology, 1992. **183**(3): p. 701-709.

30. Kelley, D.A.C., L.L. Wald, and J.M. Star-Lack, *Lactate detection at 3T: Compensating J coupling effects with BASING.* Jmri-Journal of Magnetic Resonance Imaging, 1999. **9**(5): p. 732-737.

31. Choi, C., et al., *2-hydroxyglutarate detection by magnetic resonance spectroscopy in subjects with IDH-mutated gliomas.* Nature Medicine, 2012. **18**(4): p. 624-629.

32. Dang, L., et al., *Cancer-associated IDH1 mutations produce 2-hydroxyglutarate.* Nature, 2009. **462**(7274): p. 739-U52.

33. Bottemley, P.A., *Selective volume method for performing localized NMR spectroscopy*, 1984: US.

34. Adams, J.G. and E.R. Melhem, *Clinical usefulness of T2-weighted fluid-attenuated inversion recovery MR imaging of the CNS.* AJR American Journal of Roentgenology, 1999. **172**(2): p. 529-36.

35. Ogg, R.J., P.B. Kingsley, and J.S. Taylor, *Wet, a T-1-Insensitive and B-1-Insensitive Water-Suppression Method for in-Vivo Localized H-1-Nmr Spectroscopy.* Journal of Magnetic Resonance Series B, 1994. **104**(1): p. 1-10.

36. Gruetter, R., *Automatic, Localized Invivo Adjustment of All 1st-Order and 2nd-Order Shim Coils.* Magnetic Resonance in Medicine, 1993. **29**(6): p. 804-811.

37. Naressi, A., et al., *Java-based graphical user interface for the MRUI quantitation package.* Magnetic Resonance Materials in Physics Biology and Medicine, 2001. **12**(2-3): p. 141-152.

38. Provencher, S.W., *Estimation of Metabolite Concentrations from Localized in-Vivo Proton Nmr-Spectra.* Magnetic Resonance in Medicine, 1993. **30**(6): p. 672-679.

39. Norton, W.T., S.E. Poduslo, and K. Suzuki, *Subacute Sclerosing Leukoencephalitis .2. Chemical Studies Including Abnormal Myelin and an*

Abnormal Ganglioside Pattern. Journal of Neuropathology and Experimental Neurology, 1966. **25**(4): p. 582-&.

40. Traber, F., et al., *H-1 metabolite relaxation times at 3.0 tesla: Measurements of T1 and T2 values in normal brain and determination of regional differences in transverse relaxation.* Journal of Magnetic Resonance Imaging, 2004. **19**(5): p. 537-545.

41. Li, Y., et al., *Comparison of T-1 and T-2 metabolite relaxation times in glioma and normal brain at 3T.* Journal of Magnetic Resonance Imaging, 2008. **28**(2): p. 342-350.

42. Mlynarik, V., S. Gruber, and E. Moser, *Proton T-1 and T-2 relaxation times of human brain metabolites at 3 Tesla.* Nmr in Biomedicine, 2001. **14**(5): p. 325-331.

43. Ganji, S.K., et al., *T2 measurement of J-coupled metabolites in the human brain at 3T.* Nmr in Biomedicine, 2012. **25**(4): p. 523-529.

44. Brief, E.E., et al., *Proton T-2 relaxation of cerebral metabolites of normal human brain over large TE range.* Nmr in Biomedicine, 2005. **18**(1): p. 14-18.

45. Stubbs, M., R.L. Veech, and J.R. Griffiths, *Tumor Metabolism - the Lessons of Magnetic-Resonance Spectroscopy.* Advances in Enzyme Regulation, Vol 35, 1995. **35**: p. 101-115.

46. Kayama, T., et al., *Intratumoral Oxygen-Pressure in Malignant Brain-Tumor.* Journal of Neurosurgery, 1991. **74**(1): p. 55-59.

47. Kent, C., *Regulatory enzymes of phosphatidylcholine biosynthesis: a personal perspective.* Biochimica Et Biophysica Acta-Molecular and Cell Biology of Lipids, 2005. **1733**(1): p. 53-66.

48. Babb, S.M., et al., *Oral choline increases choline metabolites in human brain.* Psychiatry Research-Neuroimaging, 2004. **130**(1): p. 1-9.

49. Usenius, J.P., et al., *Choline-Containing Compounds in Human Astrocytomas Studied by H-1-Nmr Spectroscopy in-Vivo and in-Vitro.* Journal of Neurochemistry, 1994. **63**(4): p. 1538-1543.

50. Negendank, W., *Studies of Human Tumors by Mrs - a Review.* Nmr in Biomedicine, 1992. **5**(5): p. 303-324.

51. Lange, T., et al., *Pitfalls in lactate measurements at 3T.* American Journal of Neuroradiology, 2006. **27**(4): p. 895-901.

52. Kim, J.H., et al., *3T H-1-MR spectroscopy in grading of cerebral gliomas: Comparison of short and intermediate echo time sequences.* American Journal of Neuroradiology, 2006. **27**(7): p. 1412-1418.

53. Blamire, A.M., et al., *Proton Spectroscopy of Human Stroke - Assessment of Transverse Relaxation-Times and Partial Volume Effects in Single Volume Steam Mrs.* Magnetic Resonance Imaging, 1994. **12**(8): p. 1227-1235.

54. Frahm, J., et al., *Localized Proton Nmr-Spectroscopy in Different Regions of the Human-Brain Invivo - Relaxation-Times and Concentrations of Cerebral Metabolites.* Magnetic Resonance in Medicine, 1989. **11**(1): p. 47-63.

55. Sappeymarinier, D., et al., *Proton Magnetic-Resonance Spectroscopy of Human Brain - Applications to Normal White Matter, Chronic Infarction, and Mri White Matter Signal Hyperintensities.* Magnetic Resonance in Medicine, 1992. **26**(2): p. 313-327.

56. Cady, E.B., et al., *Lactate, N-acetylaspartate, choline and creatine concentrations, and spin-spin relaxation in thalamic and occipito-parietal regions of developing human brain.* Magnetic Resonance in Medicine, 1996. **36**(6): p. 878-886.

57. Behar, K.L., et al., *Analysis of Macromolecule Resonances in H-1-Nmr Spectra of Human Brain.* Magnetic Resonance in Medicine, 1994. **32**(3): p. 294-302.

58. Ren, J.M., A.D. Sherry, and C.R. Malloy, *H-1 MRS of Intramyocellular Lipids in Soleus Muscle at 7 T: Spectral Simplification by Using Long Echo Times Without Water Suppression.* Magnetic Resonance in Medicine, 2010. **64**(3): p. 662-671.

59. Yahya, A. and B.G. Fallone, *T-2 Determination of the J-Coupled Methyl Protons of Lipids: In Vivo Ilustration With Tibial Bone Marrow at 3 T.* Journal of Magnetic Resonance Imaging, 2010. **31**(6): p. 1514-1521.

60. Choi, C., et al., *Measurement of Glycine in the Human Brain in Vivo by H-1-MRS at 3 T: Application in Brain Tumors.* Magnetic Resonance in Medicine, 2011. **66**(3): p. 609-618.

61. Kaiser, L.G., K. Young, and G.B. Matson, *Numerical simulations of localized high field H-1 MR spectroscopy.* Journal of Magnetic Resonance, 2008. **195**(1): p. 67-75.

62. Slotboom, J., A.F. Mehlkopf, and W.M.M.J. Bovee, *The Effects of Frequency-Selective Rf Pulses on J-Coupled Spin-1/2 Systems.* Journal of Magnetic Resonance Series A, 1994. **108**(1): p. 38-50.

63. Posse, S., C.A. Cuenod, and D. Lebihan, *Human Brain - Proton Diffusion Mr Spectroscopy.* Radiology, 1993. **188**(3): p. 719-725.

64. Ellegood, J., C.C. Hanstock, and C. Beaulieu, *Diffusion tensor spectroscopy (DTS) of human brain.* Magnetic Resonance in Medicine, 2006. **55**(1): p. 1-8.

65. Ellegood, J., C.C. Hanstock, and C. Beaulieu, *Trace apparent diffusion coefficients of metabolites in human brain using diffusion weighted magnetic resonance spectroscopy.* Magnetic Resonance in Medicine, 2005. **53**(5): p. 1025-1032.

Biographical Information

Akshay Madan was born in Mumbai, India in November 1988. He received his Bachelor's degree in Biomedical Engineering from Watumull Institute of Electronic Engineering and Computer Technology, Mumbai University, Mumbai, India, in June 2010. He completed an internship in Siemens Ltd in the Medical Imaging department. He then began his Graduate studies in Bioengineering at University of Texas at Arlington in spring 2011. During his graduate studies he worked as a graduate research assistant in the Advanced Imaging Research Center under the supervision of Dr. Changho Choi at UT Southwestern.